IMMUNOLOGY

Lung-innervating nociceptor sensory neurons promote pneumonic sepsis during carbapenem-resistant *Klebsiella pneumoniae* lung infection

Prabhu Raj Joshi[1], Sandeep Adhikari[1], Chinemerem Onah[1], Camille Carrier[1], Abigail Judd[1], Matthias Mack[2], Pankaj Baral[1]*

Carbapenem-resistant *Klebsiella pneumoniae* (CRKP) causes Gram-negative lung infections and fatal pneumonic sepsis for which limited therapeutic options are available. The lungs are densely innervated by nociceptor sensory neurons that mediate breathing, cough, and bronchoconstriction. The role of nociceptors in defense against Gram-negative lung pathogens is unknown. Here, we found that lung-innervating nociceptors promote CRKP pneumonia and pneumonic sepsis. Ablation of nociceptors in mice increased lung CRKP clearance, suppressed trans-alveolar dissemination of CRKP, and protected mice from hypothermia and death. Furthermore, ablation of nociceptors enhanced the recruitment of neutrophils and Ly6C^{hi} monocytes and cytokine induction. Depletion of Ly6C^{hi} monocytes, but not of neutrophils, abrogated lung and extrapulmonary CRKP clearance in ablated mice, suggesting that Ly6C^{hi} monocytes are a critical cellular population to regulate pneumonic sepsis. Further, neuropeptide calcitonin gene–related peptide suppressed the induction of reactive oxygen species in Ly6C^{hi} monocytes and their CRKP-killing abilities. Targeting nociceptor signaling could be a therapeutic approach for treating multidrug-resistant Gram-negative infection and pneumonic sepsis.

INTRODUCTION

Pneumonia and sepsis are two leading causes of hospitalizations and deaths (*1*–*3*). Gram-negative bacteria cause more than 50% of nosocomial lung infections and are a major contributor to pneumonia-induced sepsis (or pneumonic sepsis) among hospitalized patients. Carbapenem-resistant *Klebsiella pneumoniae* (CRKP) is the dominant Gram-negative lung pathogen causing fatal Gram-negative pneumonia and pneumonic sepsis (*4*, *5*). Moreover, CRKP-induced pneumonia and pneumonic sepsis are characterized by immune dysfunction, rapid bacterial outgrowth, and treatment failure due to this pathogen's broad range of antibiotic resistance including the carbapenem, one of the last antibiotic options for Gram-negative pathogens (*6*, *7*). Because of the high mortality rate (>40%) due to CRKP pneumonia in hospitalized patients, the US Centers for Disease Control and Prevention has categorized CRKP and other related members of Gram-negative bacteria as an "urgent public health threat," emphasizing the immediate and aggressive actions for the control of this pathogen (*8*–*10*). An alternative nonantibiotic treatment approach for Gram-negative pneumonia and pneumonic sepsis is essential.

The lungs are the primary site of air exchange, which results in daily inhalation of hundreds to thousands of airborne microbes, some of which are pathogens (*11*). While lung-innervating sensory neurons control the physiologic process of gas exchange, their role in coordinating the lung immune response to achieve sterilizing immunity is unknown. At homeostasis, airway-resident cells, such as alveolar macrophages (AMs) and tissue-resident T cells, sense and respond to inhaled pathogens for their clearance in the lungs and prevention of their spread in the body (*12*). Moreover, these cells rapidly produce cytokines and chemokines that regulate the entry of myeloid innate phagocytes into the airways during severe CRKP lung infections (*12*, *13*). Thus, these cells coordinate the CRKP clearance at the primary site of infection and protect the host from developing pneumonic sepsis. Neutrophils and monocytes are among the first cells migrating from blood circulation to the site of infection, where they phagocytose and kill CRKP via reactive oxygen species (ROS) production (*14*, *15*). These innate immune cells also produce cytokines and chemokines as well as several proteolytic enzymes, enhancing the further influx and activation of other immune cell types such as macrophages (*16*, *17*). Conventional natural killer cells and type 3 innate lymphoid cells (ILC3s) were also observed for the CRKP clearance from lung tissues in murine studies (*18*, *19*).

The lungs are heavily innervated by nociceptor sensory neurons (nociceptors) (*20*–*22*). These neurons are a major subset within a sensory nervous system that responds to noxious stimuli, such as heat, adenosine triphosphate (ATP), chemical irritants, inflammation, and mechanical tissue damage, to mediate neurogenic inflammation and pain (*23*–*25*). Most of the nociceptor innervation to the airways and lung parenchyma comes from the nodose and jugular ganglia [or vagal ganglia (VG)] origin, and the innervation from dorsal root ganglia (DRG) contributes minorly (*20*, *22*, *26*–*28*). Upon activation, lung-innervating nociceptor neurons mediate cough, breathing, airway hyperreactivity, and allergic inflammation (*22*, *29*–*31*). During infection and inflammatory processes, a range of mediators such as pathogen-derived molecules, lipids, and secretory products of immune cells (e.g., cytokines) can bind to the receptors expressed on nociceptors, thus activating these neurons (*24*, *32*). When activated, nociceptors release neuropeptides, including calcitonin gene–related peptide (CGRP), substance P (SP), and vasointestinal peptide (VIP) into the surrounding tissue microenvironment (*24*, *32*). Further, released neuropeptides from nociceptor nerve terminals can interact with resident and recruited immune cells via binding with their cognate heterotrimeric guanine nucleotide–binding protein–coupled receptors and can activate the downstream G_s-, G_q-, or G_i-based immunomodulating signaling pathways (*24*). The role of neuroimmune

[1]Section of Microbiology and Immunology, Division of Biology, Kansas State University, Manhattan, KS 66506, USA. [2]Department of Nephrology, Regensburg University Medical Center, Regensburg 93042, Germany.
*Corresponding author. Email: baral@ksu.edu

signaling pathway(s) in regulating the host defense against Gram-negative pneumonia and pneumonic sepsis has not been characterized.

Here, we investigated the previously unexplored role of nociceptors in immunity against CRKP pneumonic sepsis in mice. We found that the genetic ablation of nociceptor neurons in septic mice led to increased survival and maintenance of core body temperature, reduced lung bacterial load, and trans-alveolar dissemination of bacteria. Furthermore, the ablation of nociceptors enhanced the recruitment of neutrophils and Ly6C^{hi} monocytes and chemokine induction. Mechanistically, depletion of Ly6C^{hi} monocytes, but not of neutrophils, led to increased lung bacterial load and dissemination of bacteria in nociceptor-deficient mice. We thus concluded that nociceptor neurons, via suppression of Ly6C^{hi} monocyte responses, dampen the lung innate immunity against CRKP pneumonia to promote pneumonic sepsis. These findings of neuroimmune interactions enhance our knowledge and may spur therapeutic strategies for treating CRKP-induced pneumonic sepsis.

RESULTS

Nociceptor neurons suppress lung defense against CRKP pneumonia and promote pneumonic sepsis

Nociceptor neurons specifically express transient receptor potential vanilloid 1 (TRPV1) ion channel. TRPV1 is a nociceptive ion channel that responds to capsaicin, noxious heat, and protons (*33*). It marks a large proportion of both vagal and DRG nociceptor neurons (*23*, *34*, *35*). Previous studies have demonstrated that lung-innervating TRPV1$^+$ neurons alter asthmatic inflammation, bronchoconstriction, and anti-*Staphylococcus* immunity (*30*, *31*, *35*). However, the role of TRPV1$^+$ neurons in Gram-negative pneumonia, more broadly the role of nociceptor-immune interactions in host response against Gram-negative sepsis, has not been investigated. Here, we hypothesized that lung-innervating nociceptors alter the local lung immune response and sepsis outcomes in a mouse model of lethal pneumonic sepsis.

We used a conditional *Cre-LoxP* genetic strategy to ablate both vagal and DRG TRPV1$^+$ neurons in mice from birth. We bred heterozygous male *Trpv1^{Cre}* mice with female homozygous *LoxP^{DTA}* mice to generate a 50:50 mixture of nociceptor-ablated *Trpv1-Cre$^{+/-}$; DTA* (hereafter Trpv1^{DTA}) and *Trpv1-Cre$^{-/-}$; DTA* (littermate control) mice (Fig. 1A). Previous studies using *Trpv1-Cre; DTA* mice have shown ablation of TRPV1$^+$ neurons in the DRG and trigeminal ganglia in Trpv1^{DTA} mice as compared to control mice (*36*, *37*).

First, we asked whether nociceptors affect the host response in mice against CRKP pneumonia and sepsis. To induce CRKP pneumonia in mice, we used CRKP strain [American Type Culture Collection (ATCC), ART 2008133] that was originally isolated from urine. Nociceptor-ablated (Trpv1^{DTA}) and control mice were infected with the lethal dose of CRKP [10^9 colony-forming units (CFU)] intranasally (Fig. 1A). Following infection, all the control mice died (0% survival) within 50 hours postinfection (hpi) but at least 60% Trpv1^{DTA} mice survived (Fig. 1B). Further, clinical condition and disease outcomes of control infected mice were worse as compared to the Trpv1^{DTA} infected mice as judged by clinical scoring over the 36 hpi (Fig. 1C). One of the hallmarks of sepsis is the rapid drop in body temperature (below 30°C) and development of septic shock syndrome. To determine the role of nociceptors in maintaining the body temperature in septic mice, we measured the core body temperature of infected mice. While there were no differences in baseline core body temperature between Trpv1^{DTA} and control groups of mice, neuron-ablated infected mice showed better control in maintaining the homeostatic body temperature than the infected control mice at 6 hpi (mean core body temperature, 31°C versus 26°C) and 24 hpi (mean core body temperature, 33°C versus 30°C) (Fig. 1D). These results suggest an increased morbidity and septic shock syndrome in control mice following CRKP infection. Moreover, CFU analyses of whole-lung homogenates after intranasal inoculation of 10^9 CFU of CRKP bacteria resulted in $>10^8$ CFU recovery in both control and Trpv1^{DTA} mice at 50 min of postinfection, suggesting no or minor impact of the inoculation technique and neuron ablation in reaching bacteria at the lungs (fig. S1, A to C).

To determine the role of nociceptors in altering hemodynamics of shock and host defense during CRKP lung challenges and to establish which mechanism contributes to the results we observed, we performed survival experiment in Trpv1^{DTA} and littermate control mice with the administration of 10^9 CFU of heat-killed CRKP bacteria. We observed 100% survival in both Trpv1^{DTA} and control mice after the challenges of heat-killed CRKP bacteria, suggesting that the differences we observed in percentage survival after live CRKP lung infection are due to the change in antibacterial defense by nociceptor neurons (Fig. 1E). After 10^9 CFU of heat-killed CRKP challenge, we observed increased core body temperature decline and clinical sign development at 6 hours after challenge in control mice than in ablated mice, but both groups of mice recovered quickly when we examined clinical signs and core body temperature at 24 hours of postchallenges (fig. S1, D and E). These data strongly suggest that the nociceptor neurons promote the CRKP lethality via modulating the anti-CRKP host defense.

One notable pathogenic feature of pneumonic sepsis is the rapid dissemination of bacteria from the airways to blood and extrapulmonary organs (*38*). As expected, bacterial dissemination was observed as early as 6 hours of CRKP lung infection in control mice and increased further at 12 and 24 hpi as judged by CFUs recovered from blood, spleen, and liver after the infection (fig. S1F). To determine the role of nociceptors in controlling bacterial dissemination in CRKP pneumonia, we quantified the CFUs of CRKP in blood, spleen, and liver and found that Trpv1^{DTA} mice, compared to control littermates, exhibited less CRKP in the blood, spleen, and liver (Fig. 1, F to H) at 24 hpi. Moreover, nociceptor-ablated mice also showed significantly increased ability of lung CRKP clearance than the nonablated control mice as judged by the reduced number of CFUs recovered from the whole-lung homogenates and bronchoalveolar lavage fluid (BALF) from Trpv1^{DTA} mice than the CFUs from the control mice at 24 hpi (Fig. 1, I and J). To determine whether the enhanced bacterial clearance abilities of nociceptor-ablated mice also occur during hypervirulent *K. pneumoniae* (hvKp) infection with a lower dose of bacterial challenge, we infected mice intranasally with hvKp. We used hvKp (ATCC strain 43816), a carbapenem-sensitive and serotype K2 strain that has been used most extensively in mouse infection studies (*39*–*42*). Intranasal infection of mice with 10^4-CFU dose of hvKp led to minor reduction in bacterial load in the airways in nociceptor-ablated mice at 24 hpi as compared to the bacterial load in the airways from littermate control mice, but no differences were observed in the bacterial load in spleen and liver (fig. S1, G to I), suggesting a minor role of nociceptor neurons in promoting lung infection with hvKp.

In addition, reduction in CRKP CFUs in the lung, liver, and spleen in nociceptor-ablated mice was not observed at 12 hpi, indicating a possible time window needed to have an impact of neuronal signals

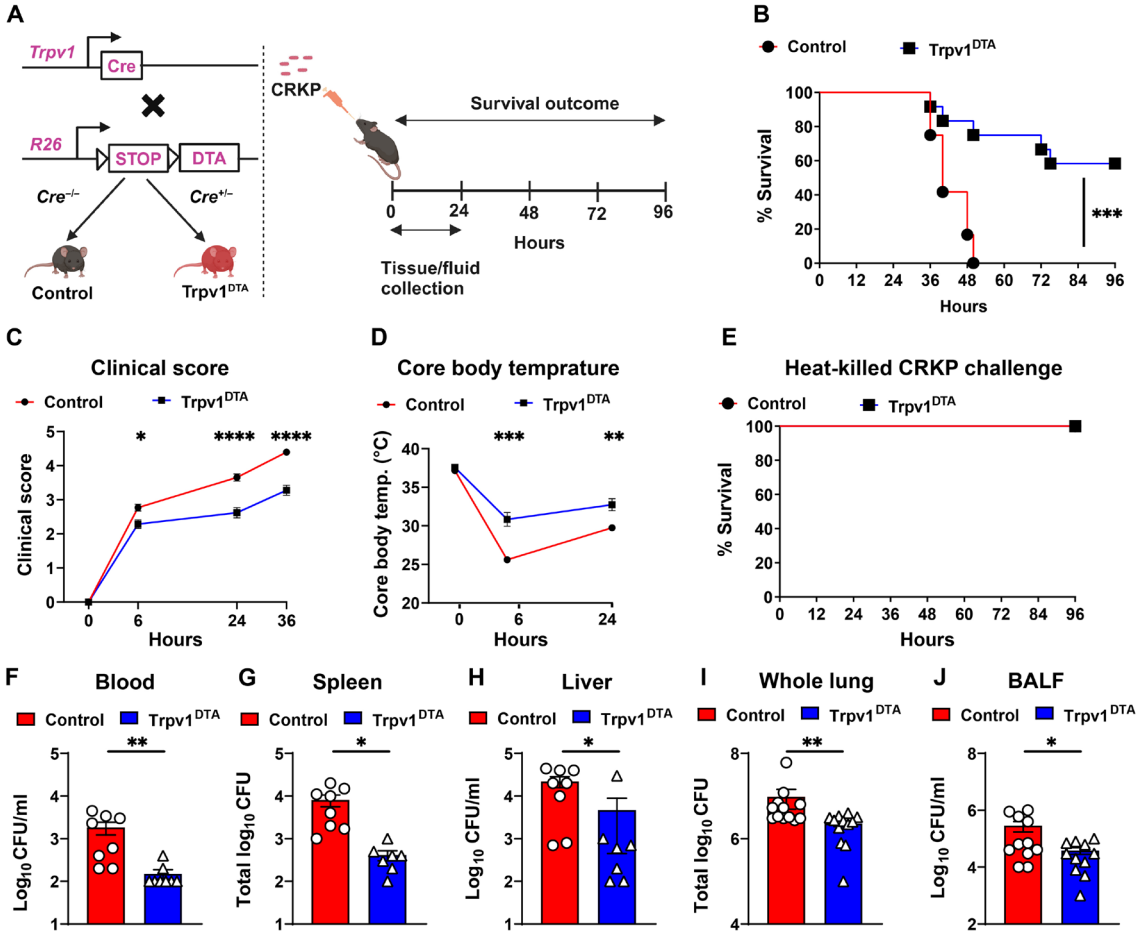

Fig. 1. Nociceptor neurons suppress host protection against CRKP pneumonia and pneumonic sepsis. (**A**) Genetic strategy for ablating TRPV1$^+$ neurons in mice (left) and mouse model of CRKP lung infection (right). Control and Trpv1^{DTA} mice were infected with the lethal dose (10^9 CFU per mouse) of CRKP intranasally. (**B** to **D**) Survival curve (B), clinical score (C), and core body temperature (D) of control and Trpv1^{DTA} mice over time. Data in (B) include Trpv1^{DTA} mice ($n = 12$) and littermate control mice ($n = 12$) from three independent experiments. Data in (C) and (D) are the means ± SEM and involve Trpv1^{DTA} mice ($n = 8$ to 12 mice per group) and control littermates ($n = 8$ to 12 mice per group). (**E**) Survival curve of control ($n = 8$) and Trpv1^{DTA} mice ($n = 8$) after intranasal challenge with heat-killed CRKP bacteria (10^9 CFU per mouse). (**F** to **J**) CFUs recovered in blood (F), spleen (G), liver (H), whole lung (I), and BALF (J) from control and Trpv1^{DTA} mice at 24 hpi. Each symbol denotes a mouse [(F) to (J)]. Data in (F) to (J) are the means ± SEM and at least two independent experiments with $n = 7$ to 12 mice per group. Statistical analysis was done by log-rank (Mantel-Cox) test [(B) and (E)], two-way analysis of variance (ANOVA) with Sidak's multiple comparison's test (C), repeated measures two-way ANOVA with Sidak's multiple comparison's test (D), Mann-Whitney test [(F), (H), and (I)], and two-tailed unpaired *t* test [(G) and (J)]. Levels of significance for all statistical analyses: *$P < 0.05$, **$P < 0.01$, ***$P < 0.001$, ****$P < 0.0001$. BioRender.com was used to create schematic in (A).

on CRKP clearance (fig. S1, J to L). The difference in the weight of spleen was not observed among Trpv1^{DTA} mice and control mice after 24 hours of CRKP lung infection (fig. S1M), suggesting that there is no noticeable difference in early systemic inflammation between Trpv1^{DTA} and control mice. Collectively, our data demonstrate that the depletion of TRPV1$^+$ nociceptors resulted in decreased CRKP burden in the lungs and controlled CRKP dissemination to extrapulmonary sites. However, depletion of nociceptors shows a minor reduction of hvKp burden in the lungs. Thus, our results demonstrate that the ablation of nociceptors protects mice from lethal CRKP pneumonia and pneumonic sepsis.

Nociceptor neurons inhibit immune recruitment during CRKP lung infection

To determine the role of nociceptors in lung damage and immune influx, we performed histopathological analysis of the lung tissues with and without CRKP infection. We performed hematoxylin and eosin (H&E) staining of lung sections from CRKP-infected lungs from control and Trpv1^{DTA} mice to determine the extent of lung damage and cellular influx at primary site of infection and parenchyma. The initial study examined whether nociceptor ablation in mice resulted in baseline changes in the lung pathology or immune cell influx. There were no noticeable differences in gross alveolar structures of the lungs at steady state between control and Trpv1^{DTA} groups of phosphate-buffered saline (PBS)–inoculated mice (Fig. 2, A and B). Also, there were no visible signs of cellular infiltration and fluid accumulation in the lungs from either group of mice (Fig. 2, A and B), suggesting that nociceptor ablation itself does not affect the overall lung morphology or cause inflammation. Next, we asked whether nociceptors regulate lung damage and cellular influx during CRKP pneumonia. By morphometric analyses, the overall lung damage, as determined by fluid accumulation and large airway

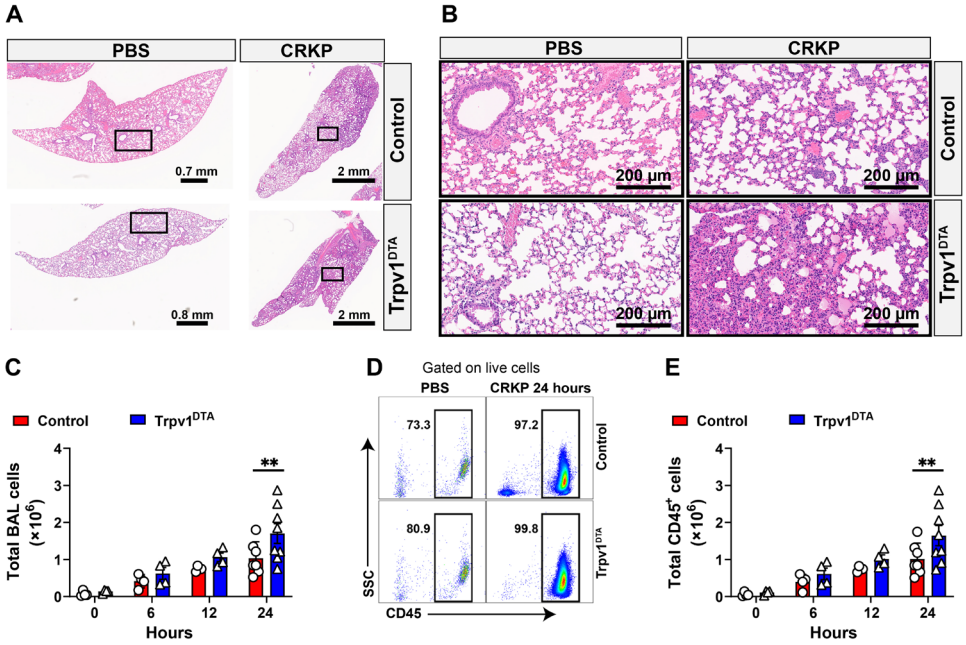

Fig. 2. Nociceptors suppress leukocyte influx during CRKP lung infection. (**A** and **B**) H&E-stained sections of lungs: ×0.9 to ×1.1 magnification (A) and ×20 magnification of selected area (in rectangles) (B) of control and Trpv1^{DTA} mice with PBS inoculation and after CRKP infection (24 hpi). Representative images were selected from at least 12 lobes of $n = 3$ to 4 mice in each group. Scale bars are shown in each figure. (**C** to **E**) Total live cells (C), representative flow cytometry plots of total leukocytes (CD45$^+$ cells) (D), and total CD45$^+$ cells (E), in BALF of Trpv1^{DTA} and control mice at 6, 12, and 24 hpi with CRKP. Data in (C) and (E) are the means ± SEM and involve $n = 4$ mice per group for 0-, 6-, and 12-hour time course analyses and $n = 7$ to 8 mice per group for 24-hour time course analyses. Statistical analysis was done by two-way ANOVA of two-stage liner step-up procedure of Benjamini, Krieger, and Yekutieli posttests with the following significance levels: $^{**}P < 0.01$. BAL, bronchoalveolar lavage.

damage/collapse, was observed similar in the lungs from nociceptor-ablated and control mice at 24 hpi (Fig. 2, A and B). In contrast, cellular infiltrates at the small size airways and lung parenchyma at 24 hpi were visibly higher in the lung sections of nociceptor-ablated mice as compared to the cellular infiltrates in lung sections from control mice (Fig. 2, A and B). Consistent with these results, we found a significantly higher number of total viable cells in the BALF isolated from nociceptor-ablated mice than the total number of cells recovered from control mice at 24 hpi (Fig. 2C). Because leukocytes are predominant cells that migrate rapidly from blood to the lungs during Gram-negative pneumonia, we hypothesized that the observed cellular difference in nociceptor-ablated and control mice is due to the difference in leukocyte transmigration. To test this hypothesis, we performed flow cytometry analysis of BALF cells and found significantly higher numbers of leukocytes (CD45$^+$ cells) in nociceptor-ablated mice than the number in control mice (Fig. 2, D and E) at 24 hpi. Together, our data suggest that the nociceptors suppress the immune recruitment into the lungs during CRKP pneumonia.

Ablation of nociceptor neurons alters the kinetics of inflammatory cytokines and chemokines

To determine the mechanism behind the increased immune infiltration in CRKP-infected nociceptor-ablated mice, we measured the levels of cytokines and chemokines in BALF at three time points (6, 12, and 24 hours) of CRKP infection. First, we measured the total BALF protein levels at these time points. The neuron-ablated Trpv1^{DTA} mice showed higher induction of total proteins in BALF at 6 hpi (Fig. 3A), and then the levels dropped at 12 and 24 hpi, suggesting that the lack of nociceptor signals augment an early inflammatory response, followed by faster resolution of inflammation. We then performed LEGENDplex cytokine/chemokine analyses at the early phase of infection (6 hpi) and later (24 hpi, time when mice were sick but had not succumbed to death). Consistent with the results of BALF total protein, we observed significantly increased levels of pro-inflammatory cytokines [tumor necrosis factor–α (TNF-α) and interleukin-6 (IL-6)] in Trpv1^{DTA} mice at 6 hpi (Fig. 3B). In contrast, the levels of these cytokines were significantly reduced at 24 hpi in Trpv1^{DTA} mice as compared to the levels in control mice (Fig. 3C). Moreover, the level of monocyte chemoattractant protein–1 (MCP-1), a chemokine that drives monocytes to the site of infection/injury, was robustly increased in the BALF of Trpv1^{DTA} mice at 24 hpi (Fig. 3C). Further, we ran the enzyme-linked immunosorbent assay (ELISA) to determine the kinetics of TNF-α, IL-6, MCP-1, and CXCL-1 (a neutrophil-attracting chemokine) in BALF of control and Trpv1^{DTA} mice. Consistent with the LEGENDplex assay, ELISA also showed higher levels of TNF-α and IL-6 in the BALF at 6 hpi and lower levels of IL-6 at 24 hpi in Trpv1^{DTA} mice (Fig. 3D). Likewise, the levels of CXCL-1 also showed a peak of induction at 6 hpi but decreased in level at 24 hpi in Trpv1^{DTA} mice (Fig. 3D). Both assays consistently showed a significant increase in BALF MCP-1 levels at 24 hpi in Trpv1^{DTA} mice than the levels in control mice (Fig. 3, C and D). The production kinetics of chemokine (C-C motif) ligand 7 (CCL7) and CXCL-5 with and without nociceptor ablation resulted in similar trend as we observed for production of CCL2 (MCP-1) and CXCL-1, respectively (Fig. 3D).

In sum, time course analyses of total proteins, TNF-α, IL-6, CXCL-1, and CXCL-5 indicated that the lack of nociceptors resulted in marked early induction of inflammatory cytokines and mediated faster resolution of inflammatory process at later time

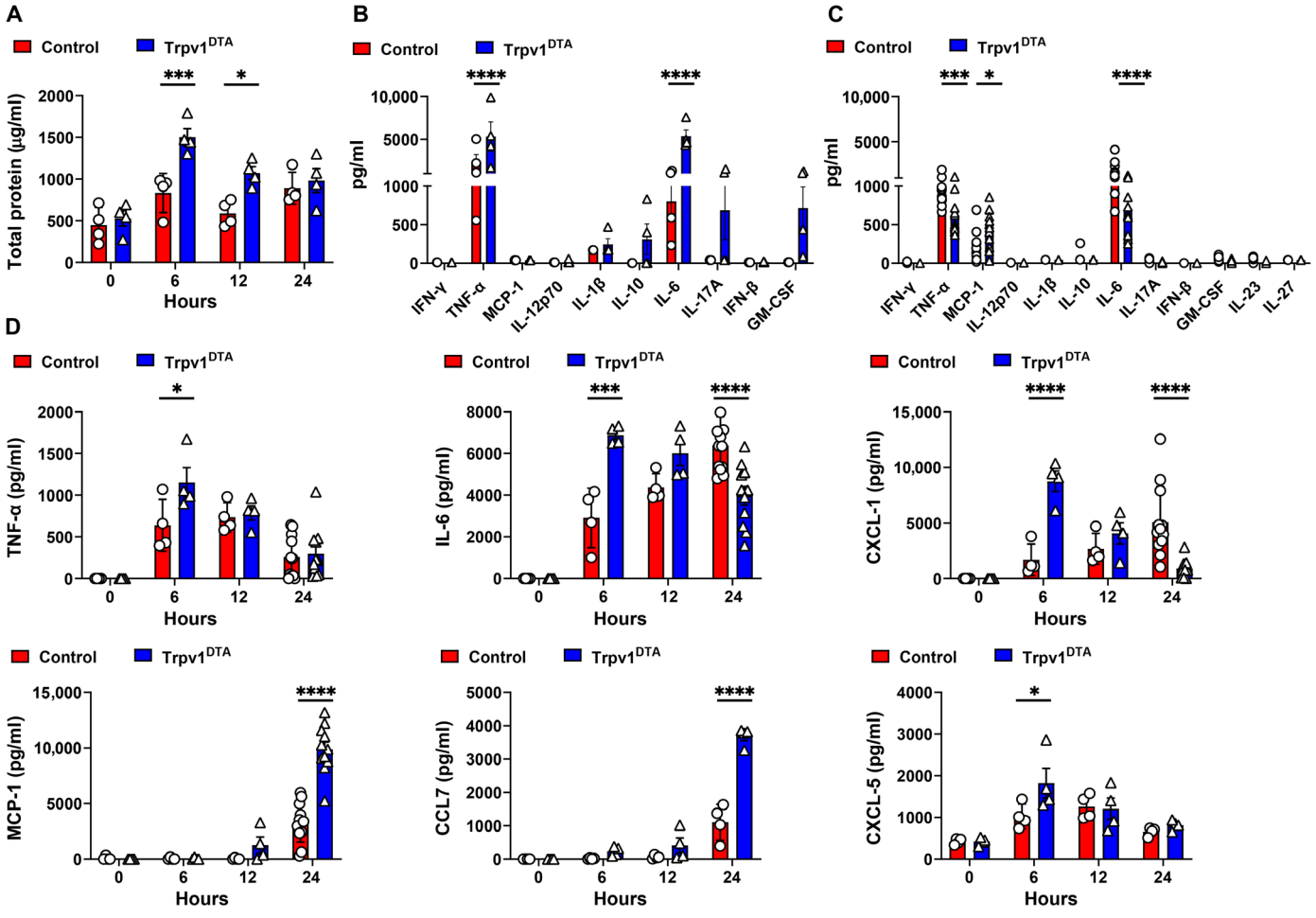

Fig. 3. Ablation of nociceptors alter the kinetics of cytokine and chemokine induction after CRKP infection. (**A**) Total proteins in BALF over time of CRKP infection. (**B** and **C**) Panels of inflammatory cytokines measured by LEGENDplex assay in BALF at 6 (B) and 24 hpi (C). (**D**) Measurement of selected cytokines and chemokines (TNF-α, IL-6, CXCL-1, MCP-1, CCL7, and CXCL-5) by ELISA in BALF over time of CRKP infection. Data in (A) to (D) are the means ± SEM and involve Trpv1^{DTA} mice ($n = 4$ mice per group for 0, 6, and 12 hours and $n = 4$ to 11 mice per group for 24 hours) and control littermates ($n = 4$ mice per group for 0, 6, and 12 hours and $n = 4$ to 12 mice per group for 24 hours). Data were analyzed by two-way ANOVA with Sidak's multiple comparison's posttests [(A) and (D)] and two-way ANOVA of two-stage liner step-up procedure of Benjamini, Krieger, and Yekutieli posttests [(B) and (C)] with the following significance levels: *$P < 0.05$, ***$P < 0.001$, ****$P < 0.0001$.

points of CRKP infection (Fig. 3D). Together, our data suggest that the lung-innervating nociceptors modulate the kinetics of airway cytokine/chemokine production during CRKP pneumonia, which might be linked to immune infiltration and bacterial clearance.

Nociceptor neurons suppress the recruitment of neutrophils, monocytes, and interstitial macrophages during CRKP infection

The CXCL (CXCL-1 and CXCL-5) and CCL (CCL2 and CCL7) chemokines are well studied chemokines that attract neutrophils and monocytes, respectively, to the site of inflammation (*43*–*45*). Thus, we hypothesize that early induction of CXCL-1 and CXCL-5 might contribute to increased neutrophil recruitment in Trpv1^{DTA} mice, whereas MCP-1 and CCL7 induction at 24 hpi contributed to monocyte recruitment. Neutrophils and monocytes have previously been reported to play a critical role in the clearance of *K. pneumoniae* from infected lungs (*15*, *17*, *46*). Therefore, we speculated that the host protection and increased bacterial clearance in Trpv1^{DTA} mice are attributed because of the higher influx of neutrophils and monocytes into the airways and lung parenchyma. To test this hypothesis, we characterized and quantified immune cell populations in BALF after CRKP infection using flow cytometry analysis (fig. S2). Flow cytometric analyses of BALF cells revealed significantly greater numbers of CD11b$^+$ Ly6G$^+$ neutrophils and CD11b$^+$ Ly6G$^-$ Ly6C$^+$ (Ly6C^{hi}) monocytes in Trpv1^{DTA} mice compared to control littermates at 24 hpi (Fig. 4, A to C). The number of AMs was significantly higher in uninfected Trpv1^{DTA} mice than the number in control mice, but their numbers rapidly decreased at 6, 12, and 24 hpi with no differences between the two groups of mice (Fig. 4, A and D). Also, the abundance of interstitial macrophages (IMs) in Trpv1^{DTA} mice considerably increased at early phase (6 hours) of infection and at 24 hpi when compared to the abundance in control mice (Fig. 4E). In addition, the numbers of CD4$^+$ T cells, B cells, CD8$^+$ T cells and non–T and non–B cells were observed similar in neuron-ablated and control mice (fig. S2, B to E). Moreover, the BALF immune cell analyses after 24 hours of hvKp infection showed an increased neutrophil number only in Trpv1^{DTA} mice, indicating the potential contribution of

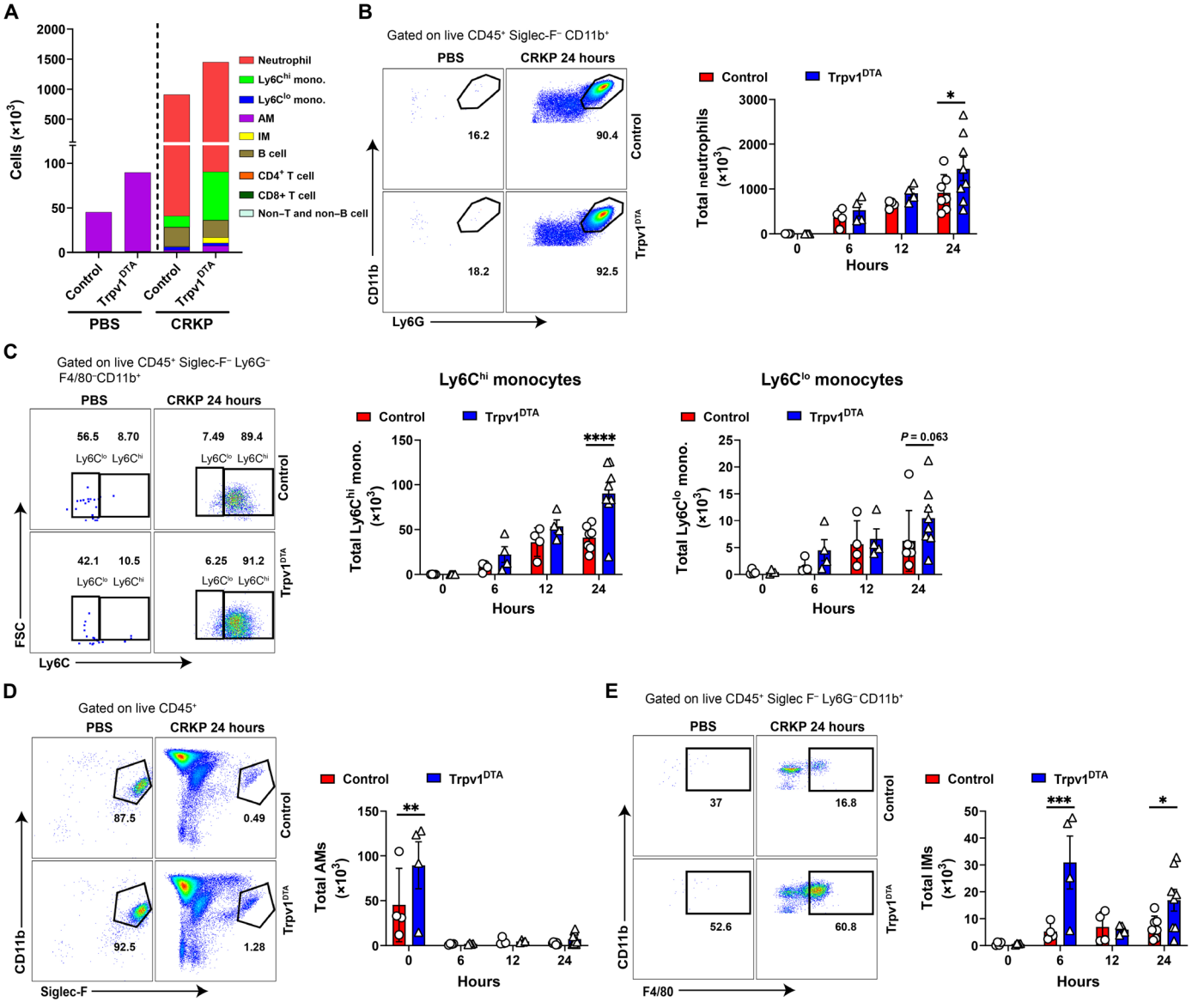

Fig. 4. Nociceptors dampen recruitment of neutrophils, monocytes, and interstitial macrophages into airways during CRKP infection. (**A**) Numbers of leukocyte subsets quantified in BALF of Trpv1^{DTA} and control littermates at 24 hpi or of PBS treatment. (**B** to **E**) Representative flow cytometry plots and absolute total numbers of neutrophils (CD11b$^+$ Ly6G$^+$) (B), Ly6C^{hi} and Ly6C^{lo} monocytes (C), AMs (Siglec-F$^+$CD11b$^-$CD11c$^+$ F4/80$^+$) (D), and interstitial macrophages (IMs; CD11b$^+$ F4/80$^+$) (E) in BALF of Trpv1^{DTA} and control mice over time after CRKP infection or PBS treatment. Data in (A) to (E) are the means ± SEM and involve Trpv1^{DTA} mice ($n = 4$ per group for 0, 6, and 12 hours and $n = 8$ per group for 24 hours) and control littermates ($n = 4$ per group for 0, 6, 12 hours and $n = 7$ per group for 24 hours). Data were analyzed by two-way ANOVA of two-stage liner step-up procedure of Benjamini, Krieger, and Yekutieli posttests with the following significance levels: *$P < 0.05$, **$P < 0.01$, ***$P < 0.001$, ****$P < 0.0001$.

neutrophils in reduced airway hvKp burden in nociceptor-ablated mice (fig. S2, F and G).

In a previous study, γδ T cells are critical in mediating protection against *Staphylococcus aureus* pneumonia in nociceptor-ablated mice (*35*). To determine whether CRKP infection increases the γδ T cell number and thereby involve in CRKP clearance, we performed CRKP infection in Trpv1^{DTA} and control mice and analyzed the abundance of total γδ T cells and other lymphoid subsets in the lungs at 24 hpi (fig. S3A). We observed an increased proportion of total γδ T cells, CD4$^+$ T cells, and IL-17A$^+$ γδ T cells in nociceptor-ablated mice as compared to the proportion in control mice (fig. S3, B and C). IL-17A has been shown to play a host protective role against carbapenem-sensitive *K. pneumoniae* lung infection by driving neutrophil influx and bacterial clearance (*42*). We did not observe any difference in IL-17A$^+$ CD4$^+$ T cells in control versus Trpv1^{DTA} mice after CRKP infection (fig. S3D). Together, our immune subsets data demonstrate the potential role of AMs, IMs, neutrophils, inflammatory monocytes (Ly6C^{hi}), γδ T cells, and CD4$^+$ T cells in mediating the rapid CRKP clearance and providing the host protection against CRKP pneumonia in nociceptor-ablated mice.

Depletion of AMs does not affect host protection against CRKP in nociceptor-ablated mice

It is possible that increased baseline abundance of AMs in Trpv1^{DTA} mice drives the recruitment of Ly6C^{hi} monocytes and neutrophils at the airspaces and confer host protection against CRKP pneumonia and sepsis. To test this idea, we performed AM depletion experiments in Trpv1^{DTA} and control mice via intratracheal treatment of clodronate liposomes (CLLs) to determine whether recruitment of monocytes and neutrophils and bacterial clearance phenotypes are reversed following CLL-dependent AM depletion. PBS liposomes (PBLs) were used as control. First, we showed that CLL-mediated AM depletion significantly decrease the AM number in CLL-treated group as compared to the number in PBL-treated group as shown in (Fig. 5, A to C, and fig. S4A). Our AM depletion strategy overall did not affect the composition of other immune cell types after the CLL treatment at baseline except some impact on IM number in CLL-treated Trpv1^{DTA} mice (fig. S4B). Next, we performed the CRKP infection experiments with and without AM depletion and still observed the increased recruitment trend of Ly6C^{hi} monocyte and neutrophils in the airways of Trpv1^{DTA} mice as compared to the numbers in control mice at 24 hpi (fig. S4, C to E). Further, the airway bacterial burden and CRKP dissemination results did not reverse with CLL-mediated AM depletion

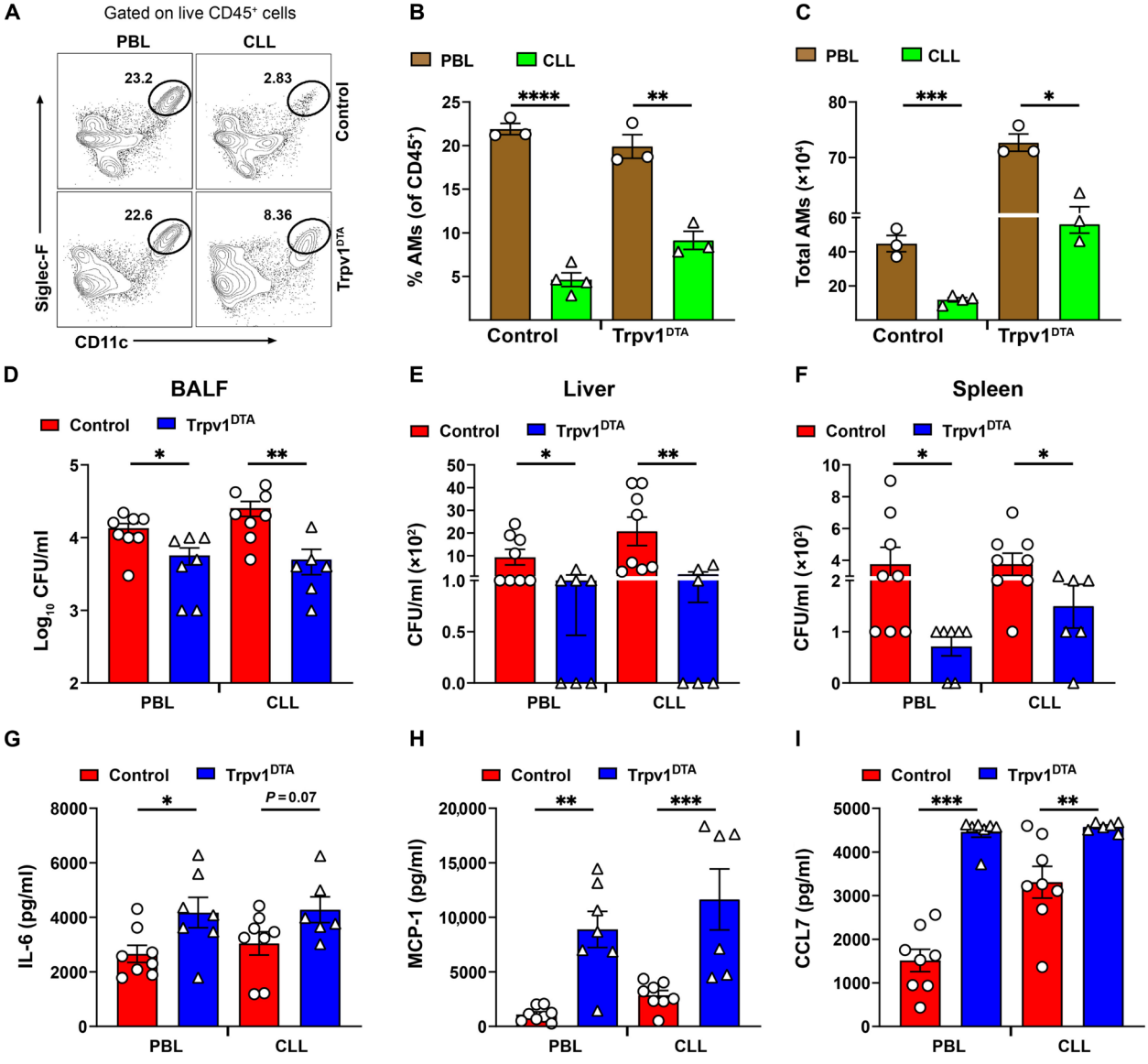

Fig. 5. Depletion of AMs does not affect host protection against CRKP in nociceptor-ablated mice. (**A**) Representative flow cytometry plots showing CLL-mediated depletion of AMs in control and Trpv1^{DTA} mice. PBL was used for control group of mice. CLL or PBL (70 μl per mouse) was inoculated via intratracheal route at 48 hours before the CRKP infection. (**B** and **C**) CLL-mediated depletion of AMs and their quantitative data at baseline after 48 hours of inoculation. (**D** to **F**) The number of CFUs recovered in BALF (D), liver (E), and spleen (F) from control and Trpv1^{DTA} mice at 24 hours CRKP after infection with and without AM depletion. (**G** to **I**) Measurement of IL-6 (G), MCP-1 (H), and CCL7 (I) in BALF of AM-depleted control and Trpv1^{DTA} mice at 24 hpi. Each symbol represents a mouse. Data in (B) to (I) are the means ± SEM. Statistical analysis was done by unpaired *t* test [(B), (C), and (G)] and Mann-Whitney test [(D) to (F) and (H) and (I)] with the following significance levels: $*P < 0.05$, $**P < 0.01$, $***P < 0.001$, $****P < 0.0001$.

in Trpv1^{DTA} versus control mice (Fig. 5, D to F). Last, cytokine and chemokine production analyses with and without AM depletion shows that the depletion of AMs in Trpv1^{DTA} mice has a minor impact on production levels of chemokines (MCP-1 and CCL7) and IL-6 (Fig. 5, G to I).

Ly6C^{hi} monocytes, but not neutrophils, are key mediators of lung CRKP clearance and to inhibit pneumonic sepsis in nociceptor-ablated mice

To elucidate the role of neutrophils and monocytes in CRKP pneumonia and pneumonic sepsis, we depleted neutrophils selectively with anti-Ly6G antibody treatment in mice and both neutrophils and monocytes via anti-GR1 antibody treatment (Fig. 6A). Depletion efficiencies of neutrophils and monocytes were analyzed by flow cytometry of BALF cells. As expected, the number of neutrophils was substantially decreased in both anti-Ly6G–treated and anti-GR1–treated mice as judged by the number of live CD11b^{+} Ly6G^{+} cells in BALF at 24 hpi (Fig. 6B). However, the numbers of live Ly6C^{hi} monocytes were only found to decrease in anti-GR1–treated mice, not in anti-Ly6G–treated mice at 24 hpi (Fig. 6, B and D). As the neutrophil subset is the dominant recruited cells (>80%) in airspaces after CRKP infection, we also found a significantly decreased number of total leukocytes (CD45^{+} cells) in anti-Ly6G– and anti-GR1–treated mice (fig. S5, A and B). Further, we also analyzed other immune cell types to determine any off-target impacts of antibody treatment. Our results showed that there is no significant impact on abundance of other immune cell types with treatment of anti-Ly6G or anti-GR1 antibodies (fig. S5, C to H).

We hypothesized that the depletion of neutrophils and/or monocytes and infection with CRKP would result in worse outcomes of mice as indicated by a rapid drop of core body temperature and increased bacterial burden and dissemination. First, we examined the core body temperature in all three treatment groups [isotype immunoglobulin G (IgG), anti-Ly6G, and anti-GR1] of mice and found that there was a reduction of core body temperature in both anti-Ly6G– and anti-GR1–treated mice when compared to the isotype IgG–treated mice. However, we observed a substantial reduction in core body temperature in isotype IgG–treated versus anti-GR1–treated mice as compared to isotype IgG-treated versus anti-Ly6G–treated mice (Fig. 6, C and E), indicating a critical role of monocytes in the maintenance of core body temperature during pneumonic sepsis. Next, we examined the CRKP load in the airways, liver, and spleen to determine whether neutrophils and/or monocytes are involved in the bacterial clearance in nociceptor-ablated mice. In isotype IgG–treated mice, as expected, we observed a significantly lower bacterial load in BALF of Trpv1^{DTA} mice than the bacterial load in control mice (Fig. 6F). Further, the bacterial load in anti-Ly6G–treated Trpv1^{DTA} mice was found significantly lower than the bacterial load in anti-Ly6G–treated control mice (Fig. 6F), suggesting that neutrophils are not playing a major role in CRKP clearance in nociceptor-ablated mice. However, the increased CRKP clearance in Trpv1^{DTA} mice was abrogated with depletion of neutrophils and monocytes in anti-GR1–treated mice (Fig. 6F), suggesting that monocytes are indispensable for the enhanced CRKP clearance in nociceptor-ablated mice. These BALF CFU data are consistent with the results of bacterial dissemination. Hence, we did not see the difference in bacterial load in the spleen and liver of isotype IgG–treated and anti-Ly6G–treated mice, but anti-GR1–treated mice showed marked increased CFUs in liver and spleen than isotype IgG– and anti-Ly6G–treated mice (Fig. 6, G and H). Furthermore, the weight of the spleen was not observed different among infected Trpv1^{DTA} and control mice that were treated with isotype IgG, anti-Ly6G, or anti-GR1 antibodies, suggesting that there was no sign of altered systemic inflammation at 24 hpi with depletion of neutrophils and/or monocytes (Fig. 6I).

We also used anti-CCR2 antibody approach to deplete Ly6C^{hi} monocytes. We administered anti-CCR2 antibody (clone MC-21) in mice, which has been used in several mouse studies for the depletion of Ly6C^{hi} CD11b^{+} monocytes (*47*–*49*). We injected a single dose of anti-CCR2 antibody at 6 hours before the CRKP infection in Trpv1^{DTA} and control mice, followed by CRKP bacterial load analyses (BALF, spleen, and liver) and BALF immune cell type analyses (Fig. 6J). As expected, we observed a significant reduction in the number of Ly6C^{hi} monocytes, but not neutrophil number, in the BALF from anti-CCR2 antibody–treated mice at 24 hpi as compared to the cell number in isotype IgG–treated mice in both Trpv1^{DTA} and control mice (Fig. 6, K and L). In isotype IgG–treated mice, we observed a significant reduction in CRKP load in the BALF and liver from Trpv1^{DTA} mice when compared to CRKP load in littermate control mice (Fig. 6, M and O). The reduced bacterial load ($P = 0.06$) was also observed in the spleen of Trpv1^{DTA} mice as compared to control mice (Fig. 6N). However, depletion of Ly6C^{hi} monocytes via anti-CCR2 antibody abrogated the reduced CRKP burden in BALF, liver, and spleen in Trpv1^{DTA} mice (Fig. 6, M to O). These findings complement with our data we observed in anti-GR1 treatment (Fig. 6, F to H). Collectively, these data suggest that Ly6C^{hi} monocytes, but not neutrophils, mediate CRKP clearance at primary site of infection and control of bacterial dissemination in Trpv1^{DTA} mice.

CRKP infection induces the release of CGRP in the airways and increases CGRP receptor on monocytes

TRPV1^{+} neurons release CGRP, a neuropeptide that was reported to play a crucial role in regulating asthmatic inflammation (*50*) and streptococcal, staphylococcal, and *Candida albicans* infections (*35*, *37*, *51*). To understand how TRPV1^{+} nociceptors promote CRKP transmigration, we analyzed CGRP levels in BALF samples from Trpv1^{DTA} and control mice. We observed significantly reduced levels of CGRP in the BALF in Trpv1^{DTA} mice compared to the levels in control mice at both baseline and with infection (Fig. 7A). Immunohistochemistry of lung tissue sections demonstrated the specific loss of lung-innervating CGRP^{+} neurons in Trpv1^{DTA} mice because we only observed the depletion of CGRP^{+} nerve fibers but not β-tubulin III–positive (TUJ1^{+}) nerve fibers in neuron-ablated mice (Fig. 7B). TUJ1 was used as a pan-neuronal nerve fiber marker and stains for both sensory and autonomic nerve fibers in the lung. Furthermore, in our BALF CGRP level measurements, we observed a robust increase in BALF CGRP levels with CRKP lung infection in control mice (Fig. 7A), suggesting a possibility of direct activation of airway TRPV1^{+} nociceptors by CRKP bacteria for neuronal activation and CGRP release. To confirm this possibility, we performed VG organotypic culture to determine whether CRKP bacteria activate the vagal nociceptors and release CGRP. We performed a time course analysis of CGRP release in VG culture following low and high doses of CRKP challenges (Fig. 7C). We found a significant CGRP release during VG stimulation with live CRKP bacteria with the peak occurring at 3 to 4 hours after stimulation (Fig. 7C). We also stimulated the VG culture with capsaicin (activates TRPV1^{+} nociceptors) as a positive control. Similar to the results in CRKP challenges, we found that capsaicin treatment significantly increased CGRP release in the culture supernatant (Fig. 7C). Together, our

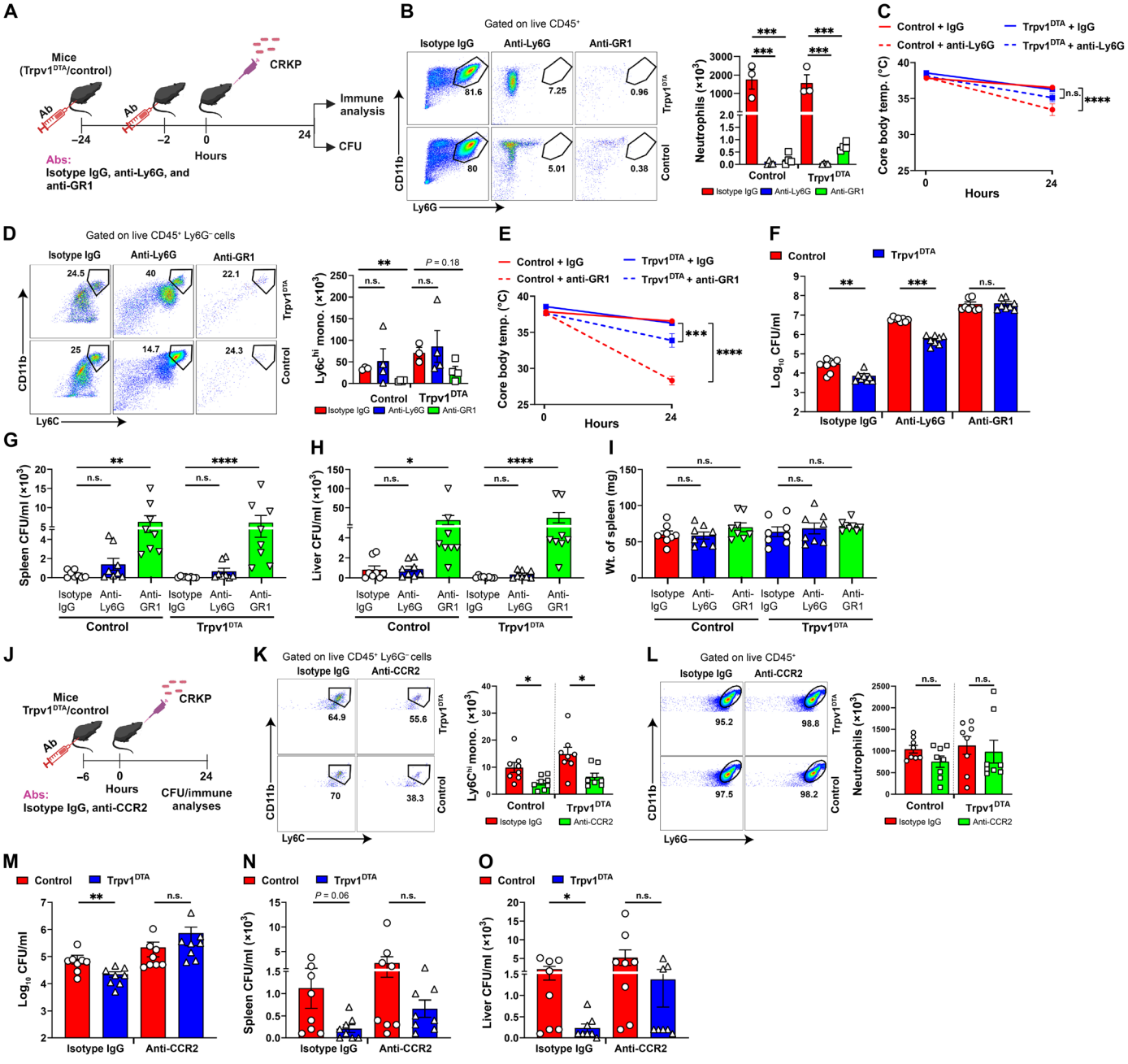

Fig. 6. Monocytes are critical for the control of CRKP dissemination and pneumonic sepsis. (**A**) Schematic showing depletion of neutrophils and monocytes and CRKP infection. (**B** and **D**) Flow cytometry plots, total neutrophils (B), and total monocytes (D) in isotype immunoglobulin G (IgG)–, anti-Ly6G–, and anti-GR1–treated control and Trpv1^{DTA} mice ($n = 3$ to 4 per group) at 24 hpi. (**C** and **E**) Core body temperature of isotype IgG–treated versus anti-Ly6G–treated mice [(C), $n = 8$ per group] and isotype IgG–treated versus anti-GR1–treated mice [(E), $n = 8$ per group] over time. n.s., not significant. (**F** to **I**) CFUs in BALF (F), spleen (G), and liver (H) and weight of spleen (I) in neutrophil/monocyte-depleted Trpv1^{DTA} and control mice ($n = 8$ per group) at 24 hpi. (**J**) Schematic showing anti-CCR2–mediated depletion of Ly6C^{hi} monocytes and CRKP infection. (**K** and **L**) Flow cytometry plots, total Ly6C^{hi} monocytes (K), and total neutrophils (L) in isotype IgG– and anti-CCR2–treated Trpv1^{DTA} and control mice ($n = 8$ per group) at 24 hpi. (**M** to **O**) CFUs in BALF (M), spleen (N), and liver (O) in monocyte-depleted Trpv1^{DTA} and control mice ($n = 8$ per group) after 24 hpi. Data in (B) to (I) and (K) to (O) are the means ± SEM. Statistical analysis: one-way ANOVA with Holm-Sidak's comparisons posttests [(B) and (I)], Brown-Forsythe and Welch ANOVA with Dunnett's T3 multiple comparisons posttests (D), repeated measures two-way ANOVA with Sidak's comparisons posttests [(C) and (E)], Mann-Whitney test [(F) and (M) to (O)], Kruskal-Wallis test with Dunn's multiple comparisons test [(G) and (H)], and unpaired t test [(K) and (L)]. Level of significance: $^{*}P < 0.05$, $^{**}P < 0.01$, $^{***}P < 0.001$, $^{****}P < 0.0001$. BioRender.com was used to create schematics in (A) and (J).

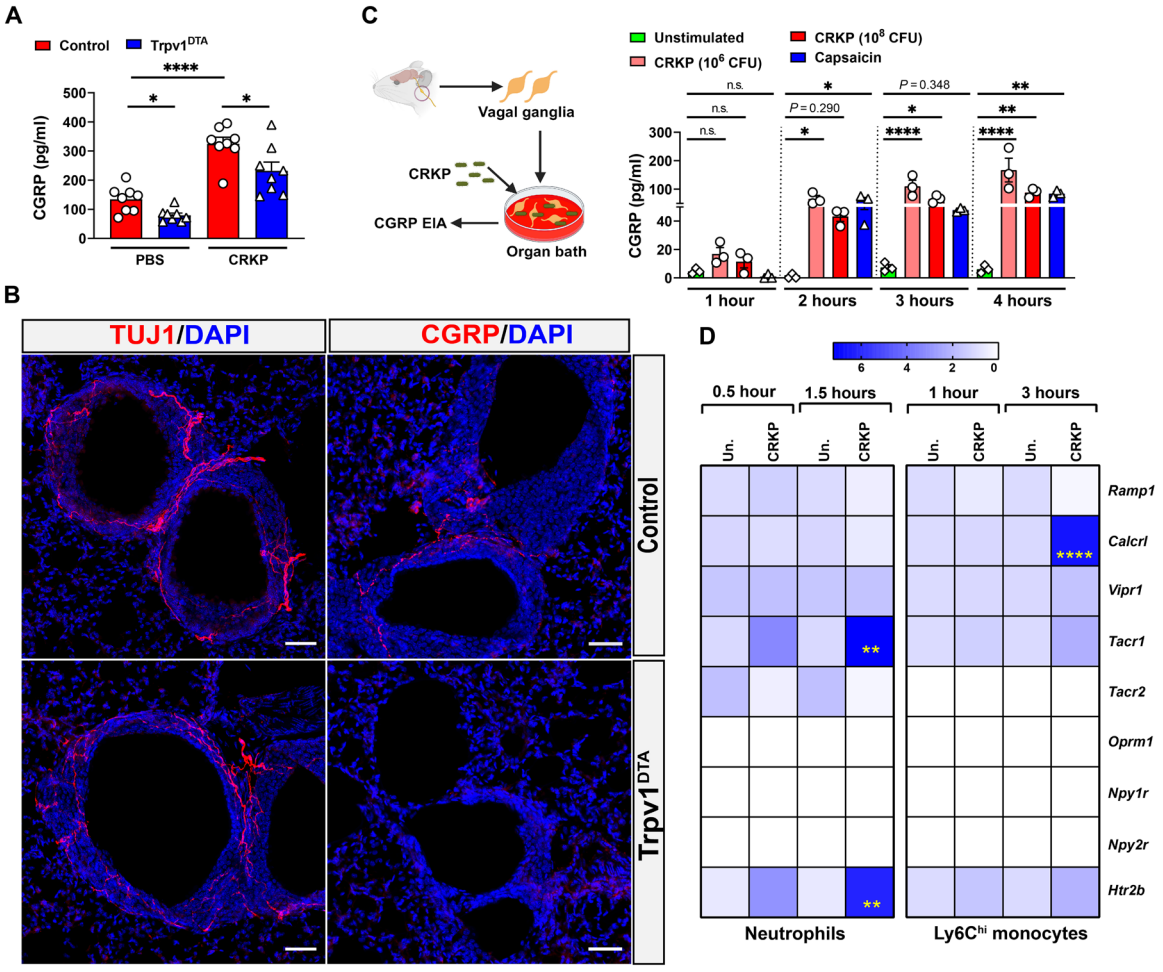

Fig. 7. CRKP infection induces the release of CGRP in the airways and the neuropeptide receptor expression by monocytes. (**A**) Levels of CGRP in BALF of PBS-treated and CRKP-infected control and Trpv1^{DTA} mice ($n = 8$ per group). (**B**) Stained sections of lungs showing β-tubulin III (TUJ1) and CGRP fibers of control and Trpv1^{DTA} mice. Representative images were selected from a total of nine images of three mice in each group (three images per mouse). Scale bars, 50 μm. DAPI, 4′,6-diamidino-2-phenylindole. (**C**) Left: Schematic showing organotypic culture of VG ($n = 4$ VGs per well) and their stimulation with CRKP to measure CGRP release. Right: Time course of CGRP release from VG culture after stimulation with CRKP bacteria (10^6 CFU per well and 10^8 CFU per well). Unstimulated wells are VG culture with media only. Capsaicin (1.5 μM) was used as positive control. (**D**) Heatmap showing relative mRNA levels of neuropeptide receptors in CRKP-infected monocytes and neutrophils at indicated time points of infection ($n \geq 3$ per group). Un., unstimulated cells. Data in (A), (C), and (D) are the means ± SEM. Statistical analysis: Brown-Forsythe and Welch ANOVA of two-stage liner step-up procedure of Benjamini, Krieger, and Yekutieli posttests (A), one-way ANOVA with Sidak's multiple comparison test (C), and two-way ANOVA with Sidak's multiple comparisons posttests (D). Level of significance: *$P < 0.05$, **$P < 0.01$, ****$P < 0.0001$. BioRender.com was used to create schematic in (C).

results demonstrate that the CRKP bacteria directly activate the vagal nociceptors and release CGRP for immunomodulation.

The CGRP receptor consists of a receptor activity modifying protein 1 (RAMP1)-calcitonin receptor-like receptor (CALCRL) heterodimer that triggers a G_s-coupled signaling pathway in immune cells (*52*). The immune-modulating role of CGRP-RAMP1 signaling has been characterized in asthma (*50*), peritonitis (*53*), streptococcal infection (*37*, *54*), and migraine pain (*55*), but it is unknown how this signaling pathway influences the CRKP lung infection and pneumonic sepsis. To determine whether neutrophils and monocytes respond to CRKP infection by increasing the expression of neuropeptide receptors including RAMP1 and CALCRL, we examined the expression levels of several neuropeptide receptor genes in purified neutrophils and Ly6C^{hi} monocytes with and without CRKP infection by quantitative polymerase chain reaction (qPCR). With our purification methods, we were able to achieve the purity of neutrophils or monocytes of >90% (fig. S6, A and D). Gene expression of *Tnf* was considered a positive control for the cell response to CRKP challenges (fig. S6, B, C, E, and F). We observed the significantly increased expression levels of the CGRP receptor gene (*Calcrl*) by Ly6C^{hi} monocytes, and SP receptor gene (*Tacr1*) and the serotonin receptor gene (*Htr2b*) by neutrophils, in response to CRKP challenges (Fig. 7D). At the baseline levels (i.e., unstimulated cells), we found the expression of several neuropeptide receptor genes by both neutrophils and monocytes, including *Ramp1*, *Calcrl*, *Vipr1* (VIP receptor gene), *Tacr1*, and *Htr2b*. Together, these findings support the hypothesis that secreted CGRP in airspaces may directly act on its heterodimer receptor complex (RAMP1/CALCRL) on recruited Ly6C^{hi} monocytes, increasing the neuroimmune signaling to dampen the antibacterial response.

CGRP-RAMP1 signaling suppresses the anti-CRKP response in Ly6C^{hi} monocytes

To understand the role of CGRP-RAMP1 signaling in CRKP infection, we performed several in vitro and in vivo experiments using the receptor-deficient (i.e., *Ramp1*$^{-/-}$ cells or mice) system, recombinant CGRP (rCGRP) treatment, and CGRP antagonist treatment. First, we determined whether rCGRP treatment in monocytes modulates the intracellular survival of CRKP. For this, we cocultured purified Ly6C^{hi} monocytes with CRKP of a multiplicity of infection (MOI) of 5 in the presence and absence of neuropeptide [CGRP, SP, VIP, and somatostatin (SST)] (Fig. 8A). Intracellular killing assay showed that the CGRP, but not other neuropeptides (SP, VIP, and SST), suppressed the monocyte-mediated killing of CRKP (Fig. 8B). In addition, CGRP also suppressed the induction of ROS within CRKP-infected monocytes (Fig. 8C). Further, CGRP-mediated suppression of intracellular bacterial killing and ROS production was abolished when we infected monocytes from *Ramp1*$^{-/-}$ mice (Fig. 8, B and C). To ascertain whether CGRP modulates the intracellular killing ability of neutrophils and macrophages, we performed cocultures of neutrophils and CRKP (MOI 5) or bone marrow–derived macrophages (BMDMs) and CRKP (MOI 5) in the presence and absence of neuropeptides (1 μM) (Fig. 8, D and F). None of the neuropeptides tested, including CGRP, affected the CRKP-killing activity of neutrophils and BMDMs (Fig. 8, E and G).

To determine the role of CGRP-RAMP1 signaling in regulation of inflammation to CRKP challenge, we examined the effect of rCGRP treatment on cytokine and chemokine production by BMDMs in response to CRKP infection. BMDMs were coincubated with CRKP (MOI 10) for 6 hours in the presence or absence of CGRP (100 nM), and cell-free supernatant was tested for cytokine measurement using ELISA and LEGENDplex assay. rCGRP treatment robustly suppressed the production of proinflammatory cytokines and chemokines including TNF-α, MCP-1, and interferon-β (IFN-β) (fig. S7, A to D), suggesting an immune inhibitory role of CGRP receptor activation in CRKP-infected macrophages.

Given that CCL chemokines (CCL2 and CCL7) are critical for monocyte recruitment in the airways during infection, we examined the cellular source of CCL chemokine. For this, we performed flow cytometric intracellular cytokine analyses of MCP-1 (CCL2) at 24 hpi. We found that leukocytes (CD45^{+} cells) are the major source of MCP-1 production during CRKP infection for both control and Trpv1^{DTA} mice (fig. S8A). Further subset analyses show that AMs, IMs, Ly6C^{hi} monocytes, and Ly6C^{low} monocytes are the major cellular sources of MCP-1 (fig. S8, A to C). It might be possible that CRKP-induced CGRP acts on lung-resident immune cells (e.g., AMs) as well as recruited cells to dampen Ly6C^{hi} monocyte responses. To test these possibilities, we isolated AMs and Ly6C^{hi} monocytes and stimulated ex vivo with CRKP in the presence and absence of rCGRP (100 nM) and found that CGRP significantly suppresses the MCP-1 production by both AM and monocyte cultures as compared to the MCP-1 production by the cultures that were not treated with CGRP (fig. S8, D and E).

To investigate the in vivo immunomodulatory role of CGRP-RAMP1 signaling in CRKP-induced pneumonic sepsis, we infected *Ramp1*$^{-/-}$ and *Ramp1*$^{+/+}$ (wild-type) mice with CRKP, followed by CFU and BALF immune subset analyses. At 24 hpi, the bacterial load in BALF was not different between *Ramp1*$^{-/-}$and WT mice (Fig. 8H). Further, flow cytometry analyses showed the higher recruitment of neutrophils (CD11b^{+}Ly6G^{+}) but not Ly6C^{hi} monocytes in *Ramp1*$^{-/-}$ mice at 24 hpi (Fig. 8I). Like the results with nociceptor ablation (fig. S2, B to E), we did not observe the differences in the number of other immune subsets at 24 hpi including B, CD4^{+} T, and CD8^{+} T cells (fig. S9, A and B). However, *Ramp1*$^{-/-}$ mice displayed higher levels of total proteins as well as cytokines TNF-α and IL-6 in the BALF as compared to WT mice (Fig. 8, J and K), suggesting that RAMP1 is critical to suppress lung inflammation and neutrophil recruitment during CRKP pneumonia but not the recruitment of Ly6C^{hi} monocytes and bacterial clearance.

To determine whether CGRP antagonism improves anti-CRKP immunity in vivo, we performed CRKP infections in CGRP antagonist ($CGRP_{8-37}$)–treated mice and PBS-treated control mice and analyzed CRKP load in the whole lungs, blood, spleen, and liver at 24 hpi (Fig. 8L). We found significantly less CRKP bacterial load in the lungs of $CGRP_{8-37}$-treated mice as compared to the CRKP load in PBS-treated control mice (Fig. 8M). Also, we observed a significant reduction in CRKP dissemination in $CGRP_{8-37}$-treated mice compared to PBS-treated mice based on CRKP number in the blood, spleen, and liver (Fig. 8, N to P). These results support the idea that nociceptor neurons, via CGRP, promote CRKP lung infection and transmigration and that blocking CGRP signaling via antagonist treatment prevents mice from developing pneumonic sepsis. Our in vivo bacterial load data observed in *Ramp1*$^{-/-}$ mice and in CGRP antagonist–treated mice do not match each other regarding the role of RAMP1 in CRKP clearance. It could be possible that the RAMP1 expression by other cell types in the lung could affect the host CRKP clearance abilities. In conclusion, our results suggest that the CRKP bacteria induce the CGRP release in the lungs and act on RAMP1/CALCRL in monocytes to suppress the bacterial killing and promote pneumonic sepsis.

DISCUSSION

Neuro-immune cross-talk has emerged as a central principle in the immune response against pathogens, both as a beneficial and detrimental regulator of anti-infection immunity (*56*). Like other barrier tissues, the respiratory tract and airways are densely innervated with nociceptor sensory neurons (or nociceptors) that mediate an array of respiratory defenses such as cough, apnea, and bronchoconstriction (*21*, *22*, *30*, *57*). Previous studies demonstrate that the activity of nociceptor neurons worsens Gram-positive bacterial infections in the lung (*35*), skin (*37*), and meninges (*54*) but protects the host from enteric *Salmonella* invasion (*58*) and skin infections with *C. albicans* (*51*) or herpes simplex virus–1 (HSV-1) (*59*), raising the question of whether tissue- or pathogen-specific neuro-immune cross-talk regulates infectious outcomes. To examine this fundamental question, we proposed to examine neuro-immune regulation in the context of CRKP pneumonia, the most common cause of Gram-negative bacterial sepsis. Herein, we found that nociceptor neurons critically regulated anti-CRKP properties of innate immune cells, particularly Ly6C^{hi} monocytes and macrophages. Furthermore, we observed that nociceptor ablation enhanced CRKP clearance in the lungs, suppressed CRKP dissemination to blood, spleen, and liver, and protected infected mice from hypothermia and death. Mechanistically, we found that nociceptors inhibit Ly6C^{hi} monocyte antibacterial responses to promote CRKP-induced sepsis, and this immunosuppressive cross-talk depends on CGRP

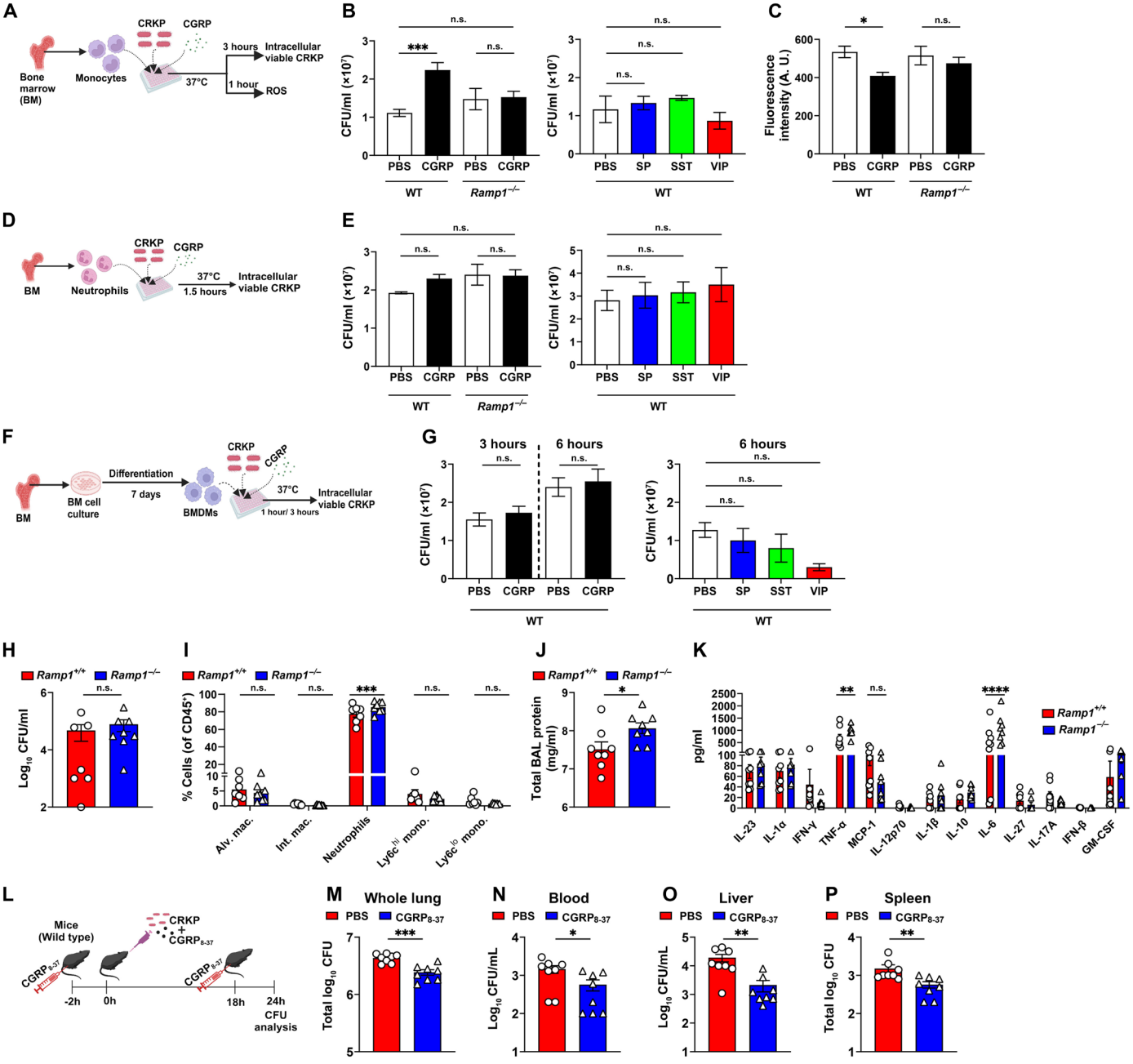

Fig. 8. CGRP-RAMP1 signaling dampens anti-CRKP response in monocytes. (**A**) Schematic showing monocyte and CRKP coculture in the presence and absence of neuropeptide. (**B** and **C**) Intracellular viable CFUs (B) and levels of ROS (C), in CRKP-infected wild-type (WT) and *Ramp*$^{-/-}$ monocytes. (**D**) Schematic of neutrophil and CRKP coculture with and without neuropeptide. (**E**) Intracellular viable CFUs in CRKP-infected WT and *Ramp*$^{-/-}$ neutrophils. (**F**) Schematic showing BMDM isolation and coculture with CRKP in the presence and absence of neuropeptides. (**G**) Intracellular viable CFUs in WT BMDMs. Data in (B), (C), (E), and (G) involve three to eight samples per group. (**H** to **K**) CRKP CFUs (H), proportions of myeloid subsets (I), total BAL protein (J), and panel of 13 mouse inflammatory cytokines/chemokines (K), measured in BALF of *Ramp1*$^{+/+}$ and *Ramp1*$^{-/-}$ mice ($n = 7$ to 8 per group) at 24 hpi. (**L**) Schematic showing administration of $CGRP_{8-37}$ (5 μg per mouse) in C57BL/6 J mice and CRKP infection. (**M** to **P**) CFUs in whole lung (M), blood (N), liver (O), and spleen (P) of PBS-treated and $CGRP_{8-37}$-treated mice ($n = 8$ per group) after 24 hpi. Data in (B), (C), (E), (G), (H) to (K) and (M) to (P) are the means ± SEM. Statistical analysis: one-way ANOVA with Sidak's multiple comparisons posttests [(B), (C), (E), and (G)], Mann-Whitney test [(H), (O), and (P)], unpaired *t* test [(J), (M), and (N)], and two-way ANOVA of two-stage liner step-up procedure of Benjamini, Krieger, and Yekutieli posttests [(I) and (K)]. Levels of significance: $*P < 0.05$, $**P < 0.01$, $***P < 0.001$, $****P < 0.0001$. BioRender.com was used to create schematics in [(A), (D), (F), and (L)].

released by neurons and on CGRP receptor expression on monocytes (Fig. 9).

A previous study showed that ablation of vagal nociceptors protected mice from lethal *S. aureus* pneumonia (*35*), and this protection involved the rapid mobilization of neutrophils from blood to the lungs for the bacterial clearance. However, in contrast with our findings, nociceptor ablation promoted higher dissemination of *S. aureus* to blood and vital organs (*35*). One explanation for these two opposing results would be the difference in the pathogenesis between *S. aureus* and CRKP. Specifically, *S. aureus* lung infection results in necrotizing pneumonia, and mortality is associated with rapid destruction of the lungs by exotoxins, but the pathogen rarely disseminates to blood and vital organs. On the other hand, Gram-negative pneumonia is characterized by rapid bacterial outgrowth and dissemination to vital organs that lead to sepsis and mortality. Host detrimental role of lung-innervating nociceptors has also been observed during *Mycobacterium tuberculosis* lung infection in guinea pigs in which nociceptor activation by *M. tuberculosis*–derived sulfolipid-1 led to the induction of cough (*57*). Such a mechanism might contribute to the airborne transmission of *M. tuberculosis* and disease spread (*57*). Similarly, a previous study also demonstrated that ablation of lung-innervating sympathetic neurons enhanced lipopolysaccharide (LPS)–induced acute lung injury or IL-33–elicited type 2 inflammation (*60*). In contrast, activation of cholinergic neurons (a subset of parasympathetic neurons) and secreted neuropeptide neuromedin U (NMU) mediated host defense against *Nippostrongylus brasiliensis* infection in the lungs and gut by triggering the host to attack the worms and expel them (*61*). In the context of fungal infection, Kaplan and colleagues (*51*, *62*) demonstrated that nociceptor neurons and secreted CGRP enhance the T helper 17 immune responses and provide protection against *C. albicans* in the skin. However, it is less understood why there are two nonexclusive modes (protective or detrimental) of neuron function in host defense against pathogens. Our results convincingly support the conclusion that lung-innervating TRPV1$^+$ nociceptors promote pneumonic sepsis due to Gram-negative bacteria via suppressing the Ly6C^{hi} monocyte responses, and ablation of these neurons leads to strong host protective responses to sepsis.

Nociceptors are known to alter the course of inflammatory response during infections. In *S. aureus* pneumonia, nociceptors ablation led to the early induction of TNF-α, IL-6, and CXCL-1 in the lungs (*35*). In HSV-1 skin infection, ablation of nociceptors showed excessive skin inflammation as indicated by elevated levels of several proinflammatory cytokines and chemokines, including IL-1β, IL-6, TNF-α, IFN- β, granulocyte-macrophage colony-stimulating factor, CXCL-1, CCL3, and MCP-1 (*59*). Consistent with these studies, we also found the induction of cytokines and chemokines including TNF-α, IL-6, CXCL-1, CXCL-5, MCP-1, and CCL7 in nociceptor-ablated mice. However, the production kinetics of these cytokines and chemokines are different at early and late phases of inflammation. Particularly, IL-6 and CXCL-1 BALF concentrations were significantly elevated at 6 hpi in ablated mice than the concentrations in control mice, but the levels sharply decreased at 24 hpi in ablated mice and were significantly lower than the control mice (Fig. 3D). Early production of TNF-α, MCP-1, IL-23, and IL-17A were shown to protect mice from *K pneumoniae* lung infection (*15*, *63*), but excessive and sustained production of TNF-α and IL-6 also causes immunopathology and mortality. Therefore, an effective immune defense mechanism against CRKP requires the host response that promotes productive innate immunity while simultaneously reducing harmful immunopathology. Our findings of an early peak of inflammatory cytokine/chemokine production, followed by rapid resolution, in nociceptor-ablated mice might be beneficial for host protection against CRKP.

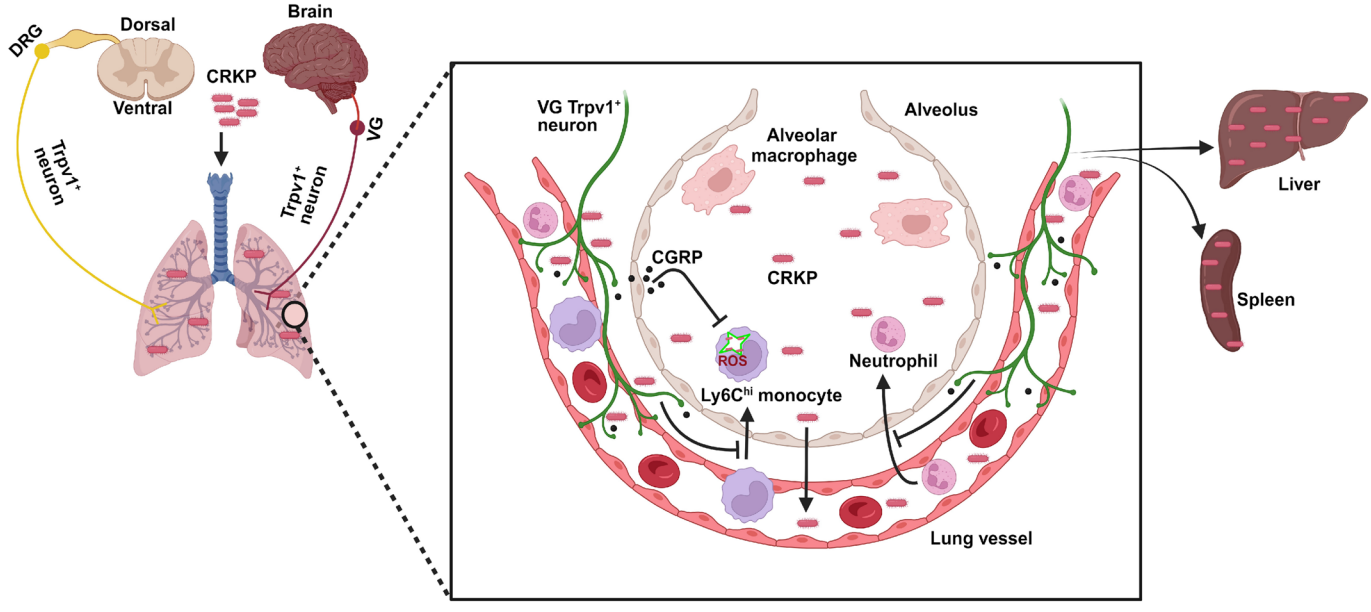

Fig. 9. Model of nociceptor regulation of CRKP-induced pneumonic sepsis. Lung-innervating nociceptor neurons suppress the recruitment of neutrophils and Ly6C^{hi} monocytes to the airspaces of lungs during CRKP lung infection. CRKP infection induces vagal TRPV1$^+$ neurons for releasing CGRP, which in turn acts on its receptor on Ly6C^{hi} monocytes to dampen the ROS production. This leads to an increased CRKP survival in the lungs and enhanced dissemination of bacteria to vital organs. BioRender.com was used to create model.

Our study has elucidated the previously uncharacterized role of nociceptors in dampening the recruitment and function of Ly6C^{hi} monocytes in the airways during Gram-negative pneumonia. Neuronal regulation of innate immune cell responses has been well recognized for neutrophils, eosinophils, macrophages, and type 2 innate lymphoid cells (ILC2s) in the lungs. In murine asthmatic lung inflammation, TRPA1^{+} and Nav1.8^{+} sensory neurons regulate the leukocyte infiltration (especially eosinophils) to the lungs and promoted allergen-induced airway inflammation and hyperreactivity (*31*, *64*). In contrast, nociceptors and sympathetic neurons reduced the influx of neutrophils into the lungs in response to *S. aureus* or LPS challenges (*35*, *60*). The neuropeptide NMU augmented the ILC2 response during *N. brasiliensis* infections (*61*). In addition, NMU also amplified inflammatory ILC2 response in allergic lung inflammation (*65*). The underlying mechanism for such variable immune cell responses is unknown, but it is possible that lung-innervating neurons influence the immune cell types based on type of inflammation (type 1 versus type 2) and stimuli (pathogen versus allergens). We went further to demonstrate nociceptive neuropeptide CGRP in regulating the function of monocytes. Our observations showed that CGRP signaling impairs intracellular ROS induction by CRKP-infected monocytes and their bactericidal abilities. On the basis of these observations, we concluded that the nociceptor-monocyte interactions negatively modulate lung immunity to CRKP pneumonic sepsis.

It is well known that the lung-resident macrophages are mainly two types: AMs and IMs. Recent studies have also shown the subsets of IMs of different functions (*66*, *67*). Our results of baseline increased abundance of AMs (Fig. 4D), and increased numbers of IMs at 6 and 24 hpi (Fig. 4E), in nociceptor-ablated mice might contribute to augmented early airway inflammation at 6 hpi and rapid resolution at 24 hpi. To support this idea, a recent study has shown a subset of IMs known as nerve-associated macrophages (NAMs, CD11b^{+}CD11c^{-}CD169^{+} IMs) that are in close proximity with sympathetic nerve fibers in the airways (*66*). NAMs were demonstrated to be distinct from AMs that highly express the tissue-reparative and anti-inflammatory genes (M2 phenotype) under steady state and during influenza A infection and provide protection against influenza-induced immunopathology (*66*). AMs may be responsible for the early inflammatory response, whereas induction of NAMs rapidly suppresses the inflammation at the latter stages of CRKP lung infection in nociceptor-ablated mice. However, AM depletion in nociceptor-ablated mice did not significantly reverse the augmented CRKP clearance, immune influx, and cytokine/chemokine production phenotypes, suggesting a role of AM-independent cell population in anti-CRKP immunity. It is possible that nociceptor regulation of AMs and recruitment of neutrophils and monocytes occur in parallel rather than in series, through distinct mechanisms. A possible mechanism for this is that nociceptors signal to other lung-resident immune cells such as γδ T cells or airway epithelial cells, which in turn could regulate monocyte/neutrophil recruitment. It is also possible that nociceptors interact with multiple tissue-resident cell populations rather than one or two cell types to modulate the inflammatory kinetics and cellular influx as a combined response. Also, we do not know the percentage of IMs that are lung resident and recruited monocyte-derived IMs in our analyses. Future work will determine whether lung-resident (e.g., NAMs) and/or monocyte-derived IMs are critical IM population downstream of nociceptors in modulating host defense against Gram-negative pneumonia.

Our results demonstrate that AMs, IMs, and Ly6C^{hi} monocytes are the dominant cell types in CRKP-infected lung for producing MCP-1/CCL2 (fig. S8). Further, CGRP significantly inhibited the MCP-1 production in ex vivo stimulation of AMs and Ly6C^{hi} monocytes with live CRKP bacterial challenges (fig. S8). Therefore, it is logical to infer that the nociceptor-mediated immunosuppression occurs via CGRP inhibitory action on both tissue-resident and recruited immune cells during CRKP pneumonia. Despite AM being one of the major cellular sources of MCP-1 production during CRKP infection, AMs are not required to control CRKP infection in nociceptor-ablated mice (Fig. 5). These results suggest the role of other MCP-1–producing cells and chemokine(s) in driving Ly6C^{hi} monocyte recruitment to control CRKP infection in nociceptor-ablated mice. Further study is needed to determine the link between nociceptors, chemokines, monocyte recruitment, and CRKP infection.

Nociceptor activation and pain sensations are critical organismic defense mechanisms to potential threats. However, our results regarding the association of nociceptor activation with enhancing CRKP infection and pneumonia lethality contradict this dogma. It is logical to assume that CRKP might use nociceptor activation as a virulent strategy to establish infection in the host. For the clearance of *Klebsiella* at the primary site of infection and mediating host protection from sepsis, rapid mobilization of Ly6C^{hi} monocytes and neutrophils at the primary site is critical. It is possible that CRKP rapidly activates the nociceptors upon infection and releases CGRP in the lungs, which might suppress the immune activation and influx of monocytes and neutrophils at primary site of infection and thereby interfere with the host bacterial clearance abilities. Such immunosuppressive role of nociceptors might be beneficial to the host during influenza virus and severe COVID-19 infection where mortality is associated with pathology and lung inflammation.

Consistent with previous studies (*35*, *54*), our study showed that the CGRP antagonist treatment enhanced anti-CRKP immunity and protected mice from sepsis. Chemical or antibody-mediated inhibition of CGRP-RAMP1/CALCRL signaling might provide therapeutic avenues for the treatment of Gram-negative pneumonia in conjunction with or as an alternative to antibiotics.

The current study has demonstrated a previously unappreciated role of nociceptor neurons in modulating lung immune response to CRKP infection. Nevertheless, some outstanding questions should be addressed by future research. First, why is nociceptor ablation associated with a strong host protective response to CRKP pneumonia but a minor protection to hvKp pneumonia? While our results show the involvement of Ly6C^{hi} monocyte in CRKP clearance and to control sepsis in nociceptor-ablated mice, nociceptor ablation has a minor impact on hvKp clearance. It is not clear what the underlying mechanism is for the two distinct mechanisms of control of pneumonia caused by carbapenem-resistant (i.e., CRKP) versus carbapenem-sensitive (i.e., hvKp) *K. pneumoniae* bacteria. One possible mechanism could be that the hvKp might use a strategy to suppress Ly6C^{hi} monocyte recruitment. Consistent with our findings, previous studies also demonstrate a distinct role CCR2^{+} Ly6C^{hi} monocytes, but not neutrophils, for clearing a carbapenem-resistant clinical isolate (Kp-MH258) of *K. pneumoniae* in mouse pneumonia studies (*15*, *46*). Their studies also demonstrate the role of neutrophils in clearing carbapenem-sensitive *K. pneumoniae* clinical isolates and hvKp 43816 strain (*15*, *46*).

Second, how do nociceptor neurons suppress the recruitment of monocytes in CRKP-infected lungs? Besides CGRP, nociceptors

also release ATP, glutamate, and other neuropeptides such as VIP, neurokinin A, and SP. An elegant strategy to address this would be single-cell RNA sequencing analyses of VGs and DRGs from CRKP-infected mice to identify previously unidentified neuropeptide(s) expressed in nociceptors during Gram-negative pneumonia and sepsis and to define their role in antibacterial signaling using genetic knockout mice or specific inhibitors.

Third, which nociceptor subset of which origin (VG, DRG, or both) regulates anti-CRKP immunity in the lungs? Our results using developmental ablation in $Trpv1^{DTA}$ mice revealed a role of nociceptor neurons in promoting pneumonic sepsis, but we do not know whether these effects are mediated by VG-specific nociceptors, DRG-specific neurons, or both. Given that VG nociceptors have been demonstrated to contribute to major innervation to the lungs (*27*, *28*), it is likely VG-specific nociceptors drive the phenotypes we observed. Previous studies showed that nociceptor neurons of VG origin regulate neutrophils and γδ T cells functions in *S. aureus* lung infection (*35*), whereas DRG nociceptors control the abundance of microfold (M) cells and numbers of segmented filamentous bacteria in the gut during *Salmonella* Typhimurium infection (*58*). Besides the involvement of lung-innervating nociceptor afferents from VG and/or DRG, vagal afferents may induce a "cholinergic anti-inflammatory reflex" via acting on vagal autonomic efferents that suppress the macrophage TNF-α production in murine endotoxemia studies (*68*, *69*).

In summary, our study has uncovered the host deleterious effects of lung-innervating nociceptors and the CGRP signaling pathway for the defense against lethal CRKP-induced pneumonic sepsis. Targeting the nociceptor neurons directly, or through downstream receptor signaling pathways in immune cells, will inform about the host-based strategy as a treatment modality for lethal Gram-negative infection and pneumonic sepsis.

MATERIALS AND METHODS

Mice

All animal experiments were approved by the Institutional Animal Care and Use Committee (IACUC 4571 and 5021), Kansas State University. Mice were housed in a pathogen-free animal facility at Kansas State University before being used for the infection model. C57BL/6 J, *Trpv1-Cre*$^{+/-}$, *loxP-DTA*$^{+/+}$, and *Ramp1*$^{+/-}$ mice were purchased from the Jackson Laboratory. *Trpv1-Cre*$^{+/-}$ mice were bred with *loxP-DTA*$^{+/+}$ to produce *Trpv1-Cre*$^{+/-}$; *DTA*$^{+/-}$ (nociceptor-ablated) and *Trpv1-Cre*$^{-/-}$; *DTA*$^{+/-}$ (littermate control). Similarly, *Ramp1*$^{+/-}$ heterozygotes were bred to generate *Ramp1*$^{-/-}$ (RAMP1 deficient) and *Ramp1*$^{+/+}$ (control littermate). Age- (8 to 10 weeks old) and sex-matched mice were used for all in vivo experiments.

Bacterial culture

Carbapenem-resistant strain of *K. pneumoniae* (CRKP, strain ART 2008133) was obtained from ATCC and used for in vivo and in vitro experiments. Hypervirulent and carbapenem-sensitive strain of *K. pneumoniae* (ATCC 43816) was also used for some experiments. The pure culture of CRKP was grown in Luria-Bertani (LB) broth for 16 hours in an Incu-shaker at 37°C and 250 rpm. The overnight culture was reinoculated into fresh LB broth and reincubated at 37°C and 250 rpm for 4.5 hours to get the bacteria in the mid-log phase. The broth culture was centrifuged at 4000 rpm for 5 min and washed with PBS (Hyclone), and an optical density of 0.5 was measured at 600 nm. Serial plating was performed on LB agar to quantify the CFUs.

Mice infection and core body temperature measurement

A mouse model of CRKP pneumonia was established by intranasal inoculation of CRKP. As in other studies, we used the lethal dose of 10^{8-9} CFUs in 35 μl of sterile PBS via intranasal instillation into mice preanesthetized with 3% isoflurane (Akron Inc.). Control mice were intranasally infused with 35 μl of sterile PBS only. Mice were kept in a microisolator and monitored four times daily for morbidity and mortality until 96 hpi. The core body temperature of the mouse was measured at 0, 6, and 24 hpi using a rectal thermal probe (Bioseb).

Clinical scoring

A person unaware of the identity of control and nociceptor-ablated mice observed and recorded the clinical conditions of mice at 0, 6, 24, and 36 hours after infection. Criteria used to evaluate the clinical conditions of mice included ruffled fur, hunched posture, shrinkage of eyes, lethargy, and labored breathing. Clinical scores 0 (normal) to 5 (moribund) were noted for each criterion. The average score of all criteria was used for statistical analysis.

Collection of BALF, tissues, and blood

Mice were euthanized with CO_2 inhalation for postmortem collection of tissue/fluid for indicated times. For BALF collection, first, a small incision was made in the neck area using the sterile scissors and forceps, and a cannula (28.5 G) was inserted into the trachea. Next, the cavities of the lungs were flushed twice with 0.8 ml of bronchoalveolar lavage buffer containing heparin (20 U/ml) (Sigma-Aldrich), dextrose (1 mg/ml) (Fisher Chemicals), and 1× PBS. A total volume of ~1.4 ml of BALF was collected in a 1.5-ml sterile Eppendorf tube. For some experiments, whole lungs, one middle lobe of liver, and whole spleen were collected aseptically in a 1.5-ml sterile Eppendorf tube. All samples were kept in ice until further processing. The areas around the eyes were wiped with 70% isopropyl alcohol swabs immediately after euthanasia of mice, and retro-orbital bleeding was done to collect blood into EDTA (1 mg/ml; BD Microtainer) containing vial. Blood samples were gently vortexed and kept in ice until further processing for CFU analysis.

Bacterial load measurement

BALF and blood samples were serially diluted with sterile 1× PBS, and diluted samples were plated onto LB agar. After the collection, whole lungs, liver, and spleen were first homogenized with BB beads (Daisy Outdoor Products) in 1 ml of sterile water using TissueLyser II (Qiagen), followed by serial dilution of samples in sterile 1× PBS. Diluted tissue lysates were plated on LB agar and incubated at 37°C overnight. Following incubation, the colonies were counted, and bacterial load was expressed as CFU per milliliter or total CFU.

H&E staining

At the indicated time points, CRKP-infected and PBS-treated mice were euthanized with CO_2 inhalation. The intact whole lung, together with the heart and trachea, was removed and kept in 15 ml of neutral buffered formalin (10%) (Sigma-Aldrich) solution at room temperature for 48 hours. The formalin-fixed tissue samples were transferred to the Veterinary Diagnostic Laboratory, Kansas State University for sectioning and H&E staining. The images were scanned using Leica Biosystems Aperio Pathology Slide Scanner. The images were processed using Aperio ImageScope software.

Total proteins and cytokine measurement

Immediately after collection, protease and phosphatase inhibitor (1%) (Thermo Fisher Scientific) was added to BALF and then aliquoted and stored at −80°C until processing for total protein analysis and cytokine measurement. Total proteins in BALF were measured using the Pierce BCA Protein Assay Kit (Thermo Fisher Scientific) according to the manufacturer's instructions. Likewise, cytokines were measured using ELISA kits (BioLegend, R&D Systems, and Abcam) and LEGENDplex assay kits (BioLegend) as per manufacturer's instructions.

BALF processing and flow cytometry analyses of BALF cells

Immune cells in the BALF were characterized and quantified by flow cytometry analyses. After the collection, BALF was immediately centrifuged at 1500 rpm for 5 min at 4°C, and the pellet was resuspended with red blood cell (RBC) lysis buffer (Thermo Fisher Scientific) for 10 min at room temperature. Cells were washed with fluorescent antibody cell sorting (FACS) buffer [PBS, 2% fetal bovine serum (FBS) (Hyclone), and 0.25 mM EDTA (RPI Research)] and centrifuged at 1500 rpm for 5 min. Cell pellets were then resuspended with 200 μl of FACS buffer. For total cell count, 10 μl of cell suspension was stained with 490 μl of trypan blue (0.04%) (Sigma-Aldrich), and viable cells were counted using a hemocytometer. For flow cytometry analyses, the cell suspensions were first transferred to the V-bottom plate, treated with FcR-blocking solution (Miltenyi Biotec), followed by incubation with antibody cocktails prepared in FACS staining buffer (1× PBS and 2% FBS) for 25 min on ice. Next, antibody-stained cells were centrifuged at 1500 rpm for 5 min at 4°C and then washed with FACS buffer and recentrifugation at 1500 rpm/4°C for 5 min. Last, stained cell pellets were resuspended with 300 μl of FACS fixative buffer (0.5 mM EDTA, 4% paraformaldehyde, and PBS) and were kept on ice until flow cytometry data acquisition. Antibodies used for staining of immune cells included the following: anti–F4/80–phycoerythrin (PE) (BioLegend), anti–B220–allophycocyanin (APC) (BioLegend), anti–CD45-APC/Cy7 (BioLegend), anti–CD11b–Brilliant Violet 650 (BioLegend), anti-CD4 Pac Blue (BioLegend), anti–CD8-PE/Cy7 (BioLegend), anti–SiglecF-Percp-Cy5.5 (BD Pharmiagen), anti–CD11c PE-Cy5 (BioLegend), anti-Ly6G Alexa Fluor 488 (BioLegend), and anti-Ly6C Brilliant Violet 785 (BioLegend). We used fluorescence minus one as a negative control to decide the appropriate gating for each immune cell characterized. To exclude dead cells, a live-cell stain (LIVE/DEAD fixable aqua, Invitrogen) or Zombie Yellow (Thermo Fisher Scientific) was used. Flow cytometry was conducted on LSRFortessa (BD) or Cytek Northern Lights flow cytometer. Data files were analyzed with FlowJo (Treestar, version 10.9).

Flow cytometry analyses of lung cells and intracellular cytokine staining

Lung tissues were mechanically separated, minced, and then digested in RPMI (Gibco) containing 2% FBS, collagenase (1.5 mg/ml; Sigma-Aldrich) and deoxyribonuclease I (30 μg/ml; Roche) at 250 rpm for 50 min at 37°C. Cells were passed through 22-gauze syringe and filtered using a 70-μM sterile filter. Following centrifugation of cell suspension at 1500 rpm for 5 min at 4°C, RBCs were lysed with 1× RBC lysis buffer (Thermo Fisher Scientific), treated with Fc receptor blocking solution (Miltenyi Biotec), and resuspended with FACS buffer (PBS, 2% FBS, and 0.25 mM EDTA/PBS). Incubation with antibody cocktails was done on ice for 30 min, and stained cells were further incubated with fixative buffer (0.5 mM EDTA, 4% paraformaldehyde, and 1× PBS) on ice for 25 min. Antibodies used to stain cells included the following: anti–CD45-APC/Cy7 (Biolegend), anti–SiglecF-Percp-Cy5.5 (BD Pharmiagen), anti–CD11c PE-Cy5 (Biolegend), anti–CD11b–Brilliant Violet 650 (Biolegend), anti-CD3 APC (Biolegend), anti-Ly6G Alexa Fluor 488 (Biolegend), and anti-Ly6C Brilliant Violet 785 (Biolegend), anti–MHC-II Alexa Fluor 700 (BioLegend), anti–B220–Brilliant Violet 510 (BioLegend), anti–NK1.1–Brilliant Violet 711 (BioLegend), anti-CD4 Pac Blue (Biolegend), anti–CD8-PE/Cy7 (Biolegend), anti–TCR-β–Alexa Fluor 700 (Biolegend), and anti–γδTCR–fluorescein isothiocyanate (BioLegend). Live cells were excluded from the Zombie Yellow–stained dead cells.

For intracellular staining of cytokines (IL-17A and MCP-1), CRKP-infected lung cells were incubated for 4 hours at 37°C with GolgiPlug (BD Biosciences). Then, the cells were stained for surface markers, fixed with Cytoperm/Cytofix Buffer (BD Biosciences) for 20 min, followed by incubation with intracellular antibodies (anti–MCP-1–PE and anti–IL-17A–PE-Dazzle 594 from BioLegend), at 1:100 in Permeabilization Buffer (BD Biosciences) for 30 min. Flow cytometry was performed using a Cytek Northern Lights flow cytometer, and data files were analyzed using FlowJo software (Treestar, version 10.9).

Depletion of neutrophils and Ly6C^{hi} monocytes

For the depletion of neutrophils and Ly6C^{hi} monocytes, we injected mice with depleting antibody as done in previous studies (*15*, *35*, *46*), with slight modification. Briefly, for neutrophil depletion, 300 μg of anti-mouse Ly6G monoclonal antibody (clone 1A8, Bio X Cell, NH) was injected into mice intraperitoneally at 24 and 2 hours before infection. Similarly, to deplete both monocytes and neutrophils, 250 μg of anti-mouse GR1 antibody (clone RB6-8C5, Bio X Cell, NH) was administered intraperitoneally into mice at 24 and 2 hours before infection. Control mice were treated with 300 μg of rat IgG2a isotype antibody (clone 2A3, Bio X Cell, NH) via intraperitoneal route at 24 and 2 hours before infection. For some experiments, we depleted Ly6C^{hi} monocytes by intraperitoneal injection of anti-CCR2 antibody (clone M-21, 30 μg per mouse) at 6 hours before infection. Control mice received rat IgG2b isotype antibody (30 μg per mouse) (clone LTF-2, Bio X Cell, NH) intraperitoneally.

Depletion of AMs

Mice were first anesthetized with a 100 mg ketamine/kg body weight (Ketaset) and 10 mg xylazine/kg body weight (Rompun) cocktail, followed by intratracheal administration of single dose of 70 μl of CLLs (Liposoma) at 48 hours before infection. Control mice were administered with PBLs (70 μl per mouse) (Liposoma).

CGRP antagonist treatment

Competitive CGRP inhibitor $CGRP_{8–37}$ (GenScript) (5 μg per mouse) was administered intraperitoneally into mice at 2 hours before infection. $CGRP_{8–37}$ (5 μg per mouse) was also challenged intranasally during CRKP infection and intraperitoneally at 18 hpi (5 μg per mouse). Control group of mice were treated with sterile 1× PBS.

VG organotypic culture for CGRP assay

For the organotypic VG culture for the CGRP release, we followed the protocol as described previously (*70*) with slight modifications. Briefly, mice were euthanized with CO_2 inhalation, and VGs were

immediately collected and stored in ice-cold Hank's buffered salt solution (Invitrogen). The isolated ganglia were transferred to a 30-mm, 0.4-μM pore size hydrophilic Millicell culture insert (Millipore-Sigma) and maintained on insert with DMEM F-12 Glutamax media (Invitrogen) supplemented with 1% penicillin/streptomycin (Invitrogen) and 20% heat-inactivated horse serum (Invitrogen). Culture media was changed every other day and maintained up to 7 days at 37°C with 5% CO_2. Then, the culture was incubated overnight with low serum (2%) containing media, followed by VG stimulation with two different doses of CRKP (1×10^6 CFU per well and 1×10^8 CFU per well). In some wells, we stimulated the culture with 1.5 μM capsaicin (Sigma-Aldrich) as positive control. Unstimulated cultures were used as negative control. Organ-free culture supernatant was collected at the indicated times and stored at −80°C before being used for the CGRP level measurements.

CGRP ELISA

BALF was collected as described in the collection of BALF section. The concentration of CGRP in the BALF and in organ free culture supernatant was determined using CGRP enzyme immunoassay kit (Novus or Cayman Chemical) according to the manufacturer's instructions.

Immunohistochemistry

Lungs were first gravity inflated with 4% PFA/PBS solution and collected into the tube containing 4% PFA/PBS solution. After overnight incubation for fixation, they were kept in 30% sucrose solutions (Fishers BioReagents) and incubated at 4°C for 48 hours. Next, they were cryo-embedded in OCT compound (Sakura Finetek) and stored at −80°C until sectioning. The 60-μM cryosections were blocked for 5 hours in PBS containing 0.3% Triton X-100 and 10% normal donkey serum (Sigma-Aldrich). Sections were then incubated with rabbit anti-β Tubulin III (Abcam) or rabbit anti-CGRP (Sigma-Aldrich) antibody at a 1:500 dilution in a solution containing 2% normal donkey serum, 0.3% Triton X-100 and 1× PBS and incubated overnight at 4°C in a rocker. After incubation, sections were incubated with donkey anti-Rabbit Alexa Flour plus 555 (secondary antibody) (Thermo Fisher Scientific) at a 1:500 dilution in a solution containing 2% normal donkey serum, 0.3% Triton X-100, and 1× PBS for 2 hours at room temperature. Sections were then transferred to the microscopic slides and then mounted with Vectashield containing 4′,6-diamidino-2-phenylindole (5 μg/ml). The antibody-stained sections were protected from light and stored at 4°C until microscopy was performed. A laser scanning confocal microscope (LSM 880 Airyscan) with Z-stack was used to capture the images of the sections.

Isolation and culture of BMDMs

Mice were first euthanized with CO_2 inhalation. Muscles were then separated to get the limb bones (tibias and femurs) and washed them with sterile 1× PBS containing 2% FBS. Bones were then crushed using a sterile mortar and pestle with sterile 1× PBS containing 2% FBS to release bone marrow (BM) cells. The BM cell suspension was passed through a 70-μM cell strainer (Cell Treat Scientific), and cells were incubated with 1× RBC lysis buffer at room temperature for 15 min, followed by washing cells twice with 1× PBS containing 2% FBS and centrifuging at 1500 rpm for 5 min at 4°C to get the cell pellet. Next, the cell pellets were suspended with DMEM containing 10% FBS. Around 10×10^6 BM cells were cultured at 37°C with 5% CO_2 in a petri plate with 10 ml of conditioned DMEM containing 20% FBS, 30% L929 cell culture supernatant (ATCC), and 1% penicillin/streptomycin (Gibco). On day 3 of incubation, an additional 10 ml of conditioned DMEM having 20% FBS, 30% L929, and 1% penicillin/streptomycin was added to the cultured cells and incubated at 37°C with 5% CO_2. On day 7, supernatant was removed from the petri plates, differentiated BMDMs were dislodged with cold 2.5 mM EDTA/PBS solution, and cells were collected in DMEM containing 10% FBS. Cell suspension was centrifuged at 1500 rpm for 5 min at 4°C, and cell pellets were resuspended with 1 to 2 ml of DMEM/10% FBS for cell counting and used for seeding into 96-well plates.

Isolation of Ly6C^{hi} monocytes and neutrophils

BM cells were isolated from mice as mentioned in BMDM isolation section. Ly6C^{hi} monocytes and neutrophils were purified from BM cells using the EasySep Mouse Monocyte Enrichment Kit (StemCell Technologies) and EasySep Mouse Neutrophil Enrichment Kit (StemCell Technologies) respectively as per manufacturer's suggestions. The purity of the Ly6C^{hi} monocytes (CD45$^+$ CD11b$^+$ Ly6C$^+$) and neutrophils (CD45$^+$ CD11b$^+$ Ly6G$^+$) was determined by flow cytometry.

Quantitative PCR

Purified monocytes (5×10^5) or neutrophils (1×10^6) were cocultured with CRKP of MOI of 5 in DMEM (Thermo Fisher Scientific) with 10% FBS. Cells were incubated at 37°C with 5% CO_2 for the indicated times, centrifuged at 1500 rpm for 5 min at 4°C for neutrophil cultures, and washed with sterile 1× PBS. Cell pellets or monolayers were lysed with TRIzol, lysates were snap frozen in dry ice and kept at −80°C. RNA was isolated using PureLink RNA Mini Kit (Thermo Fisher Scientific) and reverse transcribed to cDNA with the SuperScript II cDNA Synthesis Kit (Thermo Fisher Scientific). The relative gene expression was determined by qPCR on ABI 7000 System (Applied Biosystems) using SYBR Green Master Mix (Applied Biosystems). Primers used for gene expression analysis were used in previous studies and are listed in table S1 (*71*–*77*). The mRNA level of each gene was normalized to the expression of *Gapdh* using ΔΔ Ct method.

Intracellular killing assay

Monocytes (2×10^5 cells per well) and BMDMs (1.5×10^5 cells per well) were seeded into separate sterile 96-well (flat bottom) plates in DMEM with 10% FBS and incubated overnight at 37°C with 5% CO_2. Cells were washed once with warm sterile 1× PBS and cocultured with CRKP (MOI 5) in DMEM with 10% FBS. Neuropeptides (CGRP, SP, SST, and VIP) (Tocris Bioscience) were added in 1 μM concentration. For neutrophil killing assay, purified neutrophils (2.5×10^5 cells per well) were cocultured with CRKP (MOI 5) in the presence and absence of neuropeptides (CGRP, SP, SST, and VIP) (1 μM) in a sterile 96-well plate (U bottom) in DMEM containing 10% FBS. Cell culture plates were incubated at 37°C with 5% CO_2 for the indicated times. After incubation, monocyte and BMDM monolayers were washed twice with warm sterile PBS to remove extracellular bacteria. To remove extracellular bacteria after incubation, infected neutrophils were centrifuged at 1000 rpm for 5 min at 4°C, and cell pellets were washed twice with warm sterile PBS. Cells were lysed with 0.1% Triton X-100 (Thermo Fisher Scientific) for 15 min on ice. The cell lysate was diluted with PBS and plated on LB agar to measure the intracellular, viable bacteria.

Measurement of ROS

$Ly6C^{hi}$ monocytes were first isolated as described above and cocultured with CRKP of MOI of 5 in the presence and absence of CGRP (1 μM) at 37°C with 5% CO_2 for 3 hours. Following incubation, cells were washed with warm sterile 1× PBS and incubated with 2′, 7′-dichlorodihydrofluorescein diacetate (H_2DCFDA) (Thermo Fisher Scientific) (10 μM) for 1 hour. The fluorescence of the ROS^+ cells were measured at 488 nm using a fluorimeter (BioTek).

In vitro stimulation of BMDMs and cytokine measurement

For cytokine measurement, 1.5×10^5 BMDMs were first seeded into sterile flat-bottomed 96-well plates in DMEM containing 10% FBS and incubated at 37°C overnight with 5% CO_2. Cells were then washed with warm PBS and cocultured with CRKP of MOI of 10 with or without 100 nM CGRP for 6 hours. Cells were centrifuged at 1500 rpm for 5 min at 4°C, and the supernatant was stored at −80°C until the cytokine measurement. Measurements of cytokines and chemokines were performed using ELISA and LEGENDplex assay as per manufacturer's suggestions.

Ex vivo infection of AMs and $Ly6C^{hi}$ monocytes

For the isolation of AMs, BALF was collected from healthy C57BL/6 J mice as described in the collection of BALF section. BALF was centrifuged at 1500 rpm for 5 min at 4°C, and the cell pellet was resuspended with DMEM containing 20% FBS. $Ly6C^{hi}$ monocytes were isolated as described in the section of isolation of $Ly6C^{hi}$ monocytes. After an overnight incubation of AMs and $Ly6C^{hi}$ monocytes in sterile flat-bottomed 96-well plates in DMEM containing 10% FBS, cells were stimulated with CRKP (MOI 5) alone or CRKP (MOI 5) and CGRP (100 nM) for 6 hours at 37°C with 5% CO_2. Following centrifugation at 1500 rpm for 5 min at 4°C, cell free supernatant was collected and stored at −80°C for cytokine/chemokine measurement.

Sample size and statistical analysis

Sample size and statistical details are described in figure legends. All statistical analyses were performed using GraphPad Prism 10 software. Data were represented as means ± SEM. Mean differences of two experimental groups were compared using a two-tailed unpaired *t* test for normally distributed data. For data that were not normally distributed, Mann-Whitney test was used to compare the means of two experimental groups. Means of more than two groups were analyzed using one-way analysis of variance (ANOVA) or two-way ANOVA, as indicated in each figure legend. Means differences between experimental groups were considered statistically significant as follows: $*P < 0.05$, $**P < 0.01$, $***P < 0.001$, $****P < 0.0001$.

Supplementary Materials

This PDF file includes:

Figs. S1 to S9
Table S1

REFERENCES AND NOTES

1. J. A. Bengoechea, J. S. Pessoa, *Klebsiella pneumoniae* infection biology: Living to counteract host defences. *FEMS Microbiol. Rev.* **43**, 123–144 (2019).
2. J. P. Mizgerd, Acute lower respiratory tract infection. *N. Engl. J. Med.* **358**, 716–727 (2008).
3. C. I. Kang, J. H. Song, S. H. Kim, D. R. Chung, K. R. Peck, V. Thamlikitkul, H. Wang, T. M. So, P. R. Hsueh, R. M. Yasin, C. C. Carlos, P. H. Van, J. Perera, Risk factors and pathogenic significance of bacteremic pneumonia in adult patients with community-acquired pneumococcal pneumonia. *J. Infect.* **66**, 34–40 (2013).
4. H. Nair, E. A. Simoes, I. Rudan, B. D. Gessner, E. Azziz-Baumgartner, J. S. F. Zhang, D. R. Feikin, G. A. Mackenzie, J. C. Moiisi, A. Roca, H. C. Baggett, S. M. Zaman, R. J. Singleton, M. G. Lucero, A. Chandran, A. Gentile, C. Cohen, A. Krishnan, Z. A. Bhutta, A. Arguedas, A. W. Clara, A. L. Andrade, M. Ope, R. O. Ruvinsky, M. Hortal, J. P. McCracken, S. A. Madhi, N. Bruce, S. A. Qazi, S. S. Morris, S. El Arifeen, M. W. Weber, J. A. G. Scott, W. A. Brooks, R. F. Breiman, H. Campbell; Severe Acute Lower Respiratory Infections Working Group, Global and regional burden of hospital admissions for severe acute lower respiratory infections in young children in 2010: A systematic analysis. *Lancet* **381**, 1380–1390 (2013).
5. H. Zhang, J. Wang, W. Zhou, M. Yang, R. Wang, X. Yan, Y. Cai, Risk factors and prognosis of carbapenem-resistant *Klebsiella pneumoniae* infections in Respiratory Intensive Care Unit: A retrospective study. *Infect Drug Resist.* **14**, 3297–3305 (2021).
6. P. Y. Chung, The emerging problems of *Klebsiella pneumoniae* infections: Carbapenem resistance and biofilm formation. *FEMS Microbiol. Lett.* **363**, (2016).
7. D. M. P. De Oliveira, B. M. Forde, T. J. Kidd, P. N. A. Harris, M. A. Schembri, S. A. Beatson, D. L. Paterson, M. J. Walker, Antimicrobial resistance in ESKAPE pathogens. *Clin. Microbiol. Rev.* **33**, e00181-19 (2020).
8. Centers for Disease Control and Prevention (CDC), "2019 Antibiotic Resistance Threats Report" (U.S. Department of Health and Human Services, CDC, 2019); https://www.cdc.gov/antimicrobial-resistance/data-research/threats/?CDC_AAref_Val=https://www.cdc.gov/drugresistance/biggest-threats.html.
9. B. Suay-Garcia, M. T. Perez-Gracia, Present and future of carbapenem-resistant *Enterobacteriaceae* (CRE) infections. *Antibiotics* **8**, 122 (2019).
10. L. Xu, X. Sun, X. Ma, Systematic review and meta-analysis of mortality of patients infected with carbapenem-resistant *Klebsiella pneumoniae*. *Ann. Clin. Microbiol. Antimicrob.* **16**, 18 (2017).
11. A. Barberan, J. Ladau, J. W. Leff, K. S. Pollard, H. L. Menninger, R. R. Dunn, N. Fierer, Continental-scale distributions of dust-associated bacteria and fungi. *Proc. Natl. Acad. Sci. U.S.A* **112**, 5756–5761 (2015).
12. A. Ardain, M. J. Marakalala, A. Leslie, Tissue-resident innate immunity in the lung. *Immunology* **159**, 245–256 (2020).
13. C. Delclaux, E. Azoulay, Inflammatory response to infectious pulmonary injury. *Eur. Respir. J. Suppl.* **42**, 10s–14s (2003).
14. Z. Liang, Y. Wang, Y. Lai, J. Zhang, L. Yin, X. Yu, Y. Zhou, X. Li, Y. Song, Host defense against the infection of *Klebsiella pneumoniae*: New strategy to kill the bacterium in the era of antibiotics? *Front. Cell. Infect. Microbiol.* **12**, 1050396 (2022).
15. H. Xiong, J. W. Keith, D. W. Samilo, R. A. Carter, I. M. Leiner, E. G. Pamer, Innate lymphocyte/$Ly6C^{hi}$ monocyte crosstalk promotes *Klebsiella Pneumoniae* clearance. *Cell* **165**, 679–689 (2016).
16. C. Nathan, Neutrophils and immunity: Challenges and opportunities. *Nat. Rev. Immunol.* **6**, 173–182 (2006).
17. I. Ramirez-Moral, D. C. Blok, J. H. Bernink, M. I. Garcia-Laorden, S. Florquin, L. Boon, C. V. Veer, M. Mack, S. Saluzzo, S. Knapp, H. Spits, A. F. de Vos, T. van der Poll, Interleukin-33 improves local immunity during Gram-negative pneumonia by a combined effect on neutrophils and inflammatory monocytes. *J. Pathol.* **253**, 374–383 (2021).
18. J. P. Hoffmann, J. K. Kolls, J. E. McCombs, Regulation and function of ilc3s in pulmonary infections. *Front. Immunol.* **12**, 672523 (2021).
19. X. Xu, I. D. Weiss, H. H. Zhang, S. P. Singh, T. A. Wynn, M. S. Wilson, J. M. Farber, Conventional NK cells can produce $IL\text{-}_{22}$ and promote host defense in *Klebsiella pneumoniae* pneumonia. *J. Immunol.* **192**, 1778–1786 (2014).
20. M. Belvisi, Overview of the innervation of the lung. *Curr. Opin. Pharmacol.* **2**, 211–215 (2002).
21. K. J. Blake, X. R. Jiang, I. M. Chiu, Neuronal regulation of immunity in the skin and lungs. *Trends Neurosci.* **42**, 537–551 (2019).
22. R. B. Chang, D. E. Strochlic, E. K. Williams, B. D. Umans, S. D. Liberles, Vagal sensory neuron subtypes that differentially control breathing. *Cell* **161**, 622–633 (2015).
23. A. I. Basbaum, D. M. Bautista, G. Scherrer, D. Julius, Cellular and molecular mechanisms of pain. *Cell* **139**, 267–284 (2009).
24. P. Baral, S. Udit, I. M. Chiu, Pain and immunity: Implications for host defence. *Nat. Rev. Immunol.* **19**, 433–447 (2019).
25. A. E. Dubin, A. Patapoutian, Nociceptors: The sensors of the pain pathway. *J. Clin. Invest.* **120**, 3760–3772 (2010).
26. S. B. Mazzone, B. J. Undem, Vagal afferent innervation of the airways in health and disease. *Physiol. Rev.* **96**, 975–1024 (2016).
27. M. Tamari, K. L. Del Bel, A. M. Ver Heul, L. Zamidar, K. Orimo, M. Hoshi, A. M. Trier, H. Yano, T. L. Yang, C. M. Biggs, K. Motomura, R. Shibuya, C. D. Yu, Z. Xie, H. Iriki, Z. Wang, K. Auyeung, G. Damle, D. Demircioglu, J. K. Gregory, D. Hasson, J. Dai, R. B. Chang, H. Morita, K. Matsumoto, S. Jain, S. Van Dyken, J. D. Milner, D. Bogunovic, H. Hu, D. Artis, S. E. Turvey, B. S. Kim, Sensory neurons promote immune homeostasis in the lung. *Cell* **187**, 44–61 e17 (2024).
28. Y. Su, J. Barr, A. Jaquish, J. Xu, J. M. Verheyden, X. Sun, Identification of lung innervating sensory neurons and their target specificity. *Am. J. Physiol. Lung Cell Mol. Physiol.* **322**, L50–L63 (2022).

29. B. J. Canning, N. Mori, S. B. Mazzone, Vagal afferent nerves regulating the cough reflex. *Respir. Physiol. Neurobiol.* **152**, 223–242 (2006).
30. D. Trankner, N. Hahne, K. Sugino, M. A. Hoon, C. Zuker, Population of sensory neurons essential for asthmatic hyperreactivity of inflamed airways. *Proc. Natl. Acad. Sci. U.S.A.* **111**, 11515–11520 (2014).
31. S. Talbot, R. E. Abdulnour, P. R. Burkett, S. Lee, S. J. Cronin, M. A. Pascal, C. Laedermann, S. L. Foster, J. V. Tran, N. Lai, I. M. Chiu, N. Ghasemlou, M. DiBiase, D. Roberson, C. Von Hehn, B. Agac, O. Haworth, H. Seki, J. M. Penninger, V. K. Kuchroo, B. P. Bean, B. D. Levy, C. J. Woolf, Silencing nociceptor neurons reduces allergic airway inflammation. *Neuron* **87**, 341–354 (2015).
32. F. A. Pinho-Ribeiro, W. A. Verri Jr., I. M. Chiu, Nociceptor sensory neuron-immune interactions in pain and inflammation. *Trends Immunol.* **38**, 5–19 (2017).
33. D. Julius, TRP channels and pain. *Annu. Rev. Cell Dev. Biol.* **29**, 355–384 (2013).
34. I. M. Chiu, L. B. Barrett, E. K. Williams, D. E. Strochlic, S. Lee, A. D. Weyer, S. Lou, G. S. Bryman, D. P. Roberson, N. Ghasemlou, C. Piccoli, E. Ahat, V. Wang, E. J. Cobos, C. L. Stucky, Q. Ma, S. D. Liberles, C. J. Woolf, Transcriptional profiling at whole population and single cell levels reveals somatosensory neuron molecular diversity. *eLife* **3**, e04660 (2014).
35. P. Baral, B. D. Umans, L. Li, A. Wallrapp, M. Bist, T. Kirschbaum, Y. Wei, Y. Zhou, V. K. Kuchroo, P. R. Burkett, B. G. Yipp, S. D. Liberles, I. M. Chiu, Nociceptor sensory neurons suppress neutrophil and γδ T cell responses in bacterial lung infections and lethal pneumonia. *Nat. Med.* **24**, 417–426 (2018).
36. S. K. Mishra, S. M. Tisel, P. Orestes, S. K. Bhangoo, M. A. Hoon, $TRPV_1$-lineage neurons are required for thermal sensation. *EMBO J.* **30**, 582–593 (2011).
37. F. A. Pinho-Ribeiro, B. Baddal, R. Haarsma, M. O'Seaghdha, N. J. Yang, K. J. Blake, M. Portley, W. A. Verri, J. B. Dale, M. R. Wessels, I. M. Chiu, Blocking neuronal signaling to immune cells treats streptococcal invasive infection. *Cell* **173**, 1083–1097. e1022 (2018).
38. L. D. J. Bos, L. B. Ware, Acute respiratory distress syndrome: Causes, pathophysiology, and phenotypes. *Lancet* **400**, 1145–1156 (2022).
39. S. Cai, S. Batra, L. Shen, N. Wakamatsu, S. Jeyaseelan, Both TRIF- and MyD88-dependent signaling contribute to host defense against pulmonary *Klebsiella* infection. *J. Immunol.* **183**, 6629–6638 (2009).
40. S. Cai, S. Paudel, L. Jin, L. Ghimire, C. M. Taylor, N. Wakamatsu, D. Bhattarai, S. Jeyaseelan, NLRP6 modulates neutrophil homeostasis in bacterial pneumonia-derived sepsis. *Mucosal Immunol.* **14**, 574–584 (2021).
41. A. L. Steichen, B. J. Binstock, B. B. Mishra, J. Sharma, C-type lectin receptor $Clec_4d$ plays a protective role in resolution of Gram-negative pneumonia. *J. Leukoc. Biol.* **94**, 393–398 (2013).
42. P. Ye, F. H. Rodriguez, S. Kanaly, K. L. Stocking, J. Schurr, P. Schwarzenberger, P. Oliver, W. Huang, P. Zhang, J. Zhang, J. E. Shellito, G. J. Bagby, S. Nelson, K. Charrier, J. J. Peschon, J. K. Kolls, Requirement of interleukin 17 receptor signaling for lung CXC chemokine and granulocyte colony-stimulating factor expression, neutrophil recruitment, and host defense. *J. Exp. Med.* **194**, 519–527 (2001).
43. K. V. Sawant, K. M. Sepuru, E. Lowry, B. Penaranda, C. W. Frevert, R. P. Garofalo, K. Rajarathnam, Neutrophil recruitment by chemokines $Cxcl_1$/KC and $Cxcl_2$/MIP_2: Role of $Cxcr_2$ activation and glycosaminoglycan interactions. *J. Leukoc. Biol.* **109**, 777–791 (2021).
44. N. V. Serbina, C. Shi, E. G. Pamer, Monocyte-mediated immune defense against murine *Listeria monocytogenes* infection. *Adv. Immunol.* **113**, 119–134 (2012).
45. C. L. Tsou, W. Peters, Y. Si, S. Slaymaker, A. M. Aslanian, S. P. Weisberg, M. Mack, I. F. Charo, Critical roles for CCR_2 and $MCP\text{-}_3$ in monocyte mobilization from bone marrow and recruitment to inflammatory sites. *J. Clin. Invest.* **117**, 902–909 (2007).
46. H. Xiong, R. A. Carter, I. M. Leiner, Y. W. Tang, L. Chen, B. N. Kreiswirth, E. G. Pamer, Distinct contributions of neutrophils and $CCR2^+$ monocytes to pulmonary clearance of different *Klebsiella pneumoniae* strains. *Infect. Immun.* **83**, 3418–3427 (2015).
47. M. Mack, J. Cihak, C. Simonis, B. Luckow, A. E. Proudfoot, J. Plachy, H. Bruhl, M. Frink, H. J. Anders, V. Vielhauer, J. Pfirstinger, M. Stangassinger, D. Schlondorff, Expression and characterization of the chemokine receptors CCR_2 and CCR_5 in mice. *J. Immunol.* **166**, 4697–4704 (2001).
48. H. Liang, L. Deng, Y. Hou, X. Meng, X. Huang, E. Rao, W. Zheng, H. Mauceri, M. Mack, M. Xu, Y. X. Fu, R. R. Weichselbaum, Host STING-dependent MDSC mobilization drives extrinsic radiation resistance. *Nat. Commun.* **8**, 1736 (2017).
49. J. M. Fox, V. Roy, B. M. Gunn, L. Huang, M. A. Edeling, M. Mack, D. H. Fremont, B. J. Doranz, S. Johnson, G. Alter, M. S. Diamond, Optimal therapeutic activity of monoclonal antibodies against chikungunya virus requires Fc-FcγR interaction on monocytes. *Sci. Immunol.* **4**, eaav5062 (2019).
50. A. Wallrapp, P. R. Burkett, S. J. Riesenfeld, S. J. Kim, E. Christian, R. E. Abdulnour, P. I. Thakore, A. Schnell, C. Lambden, R. H. Herbst, P. Khan, K. Tsujikawa, R. J. Xavier, I. M. Chiu, B. D. Levy, A. Regev, V. K. Kuchroo, Calcitonin gene-related peptide negatively regulates alarmin-driven type 2 innate lymphoid cell responses. *Immunity* **51**, 709–723 e6 (2019).
51. S. W. Kashem, M. S. Riedl, C. Yao, C. N. Honda, L. Vulchanova, D. H. Kaplan, Nociceptive sensory fibers drive interleukin-23 production from $CD301b^+$ dermal dendritic cells and drive protective cutaneous immunity. *Immunity* **43**, 515–526 (2015).
52. D. R. Poyner, P. M. Sexton, I. Marshall, D. M. Smith, R. Quirion, W. Born, R. Muff, J. A. Fischer, S. M. Foord, International Union of Pharmacology. XXXII. The mammalian calcitonin gene-related peptides, adrenomedullin, amylin, and calcitonin receptors. *Pharmacol. Rev.* **54**, 233–246 (2002).
53. G. Jusek, D. Reim, K. Tsujikawa, B. Holzmann, Deficiency of the CGRP receptor component RAMP1 attenuates immunosuppression during the early phase of septic peritonitis. *Immunobiology* **217**, 761–767 (2012).
54. F. A. Pinho-Ribeiro, L. Deng, D. V. Neel, O. Erdogan, H. Basu, D. Yang, S. Choi, A. J. Walker, S. Carneiro-Nascimento, K. He, G. Wu, B. Stevens, K. S. Doran, D. Levy, I. M. Chiu, Bacteria hijack a meningeal neuroimmune axis to facilitate brain invasion. *Nature* **615**, 472–481 (2023).
55. J. C. Ray, M. Kapoor, R. J. Stark, S. J. Wang, L. Bendtsen, M. Matharu, E. J. Hutton, Calcitonin gene related peptide in migraine: Current therapeutics, future implications and potential off-target effects. *J. Neurol. Neurosurg. Psychiatry* **92**, 1325–1334 (2021).
56. H. Veiga-Fernandes, D. Mucida, Neuro-immune interactions at barrier surfaces. *Cell* **165**, 801–811 (2016).
57. C. R. Ruhl, B. L. Pasko, H. S. Khan, L. M. Kindt, C. E. Stamm, L. H. Franco, C. C. Hsia, M. Zhou, C. R. Davis, T. Qin, L. Gautron, M. D. Burton, G. L. Mejia, D. K. Naik, G. Dussor, T. J. Price, M. U. Shiloh, *Mycobacterium tuberculosis* sulfolipid-1 activates nociceptive neurons and induces cough. *Cell* **181**, 293–305 e11 (2020).
58. N. Y. Lai, M. A. Musser, F. A. Pinho-Ribeiro, P. Baral, A. Jacobson, P. Ma, D. E. Potts, Z. Chen, D. Paik, S. Soualhi, Y. Yan, A. Misra, K. Goldstein, V. N. Lagomarsino, A. Nordstrom, K. N. Sivanathan, A. Wallrapp, V. K. Kuchroo, R. Nowarski, M. N. Starnbach, H. Shi, N. K. Surana, D. An, C. Wu, J. R. Huh, M. Rao, I. M. Chiu, Gut-innervating nociceptor neurons regulate peyer's patch microfold cells and SFB levels to mediate *Salmonella* host defense. *Cell* **180**, 33–49 e22 (2020).
59. J. Filtjens, A. Roger, L. Quatrini, E. Wieduwild, J. Gouilly, G. Hoeffel, R. Rossignol, C. Daher, G. Debroas, S. Henri, C. M. Jones, B. Malissen, L. K. Mackay, A. Moqrich, F. R. Carbone, S. Ugolini, Nociceptive sensory neurons promote CD8 T cell responses to HSV-1 infection. *Nat. Commun.* **12**, 2936 (2021).
60. T. Liu, L. Yang, X. Han, X. Ding, J. Li, J. Yang, Local sympathetic innervations modulate the lung innate immune responses. *Sci. Adv.* **6**, eaay1497 (2020).
61. V. Cardoso, J. Chesne, H. Ribeiro, B. Garcia-Cassani, T. Carvalho, T. Bouchery, K. Shah, N. L. Barbosa-Morais, N. Harris, H. Veiga-Fernandes, Neuronal regulation of type 2 innate lymphoid cells via neuromedin U. *Nature* **549**, 277–281 (2017).
62. J. A. Cohen, T. N. Edwards, A. W. Liu, T. Hirai, M. R. Jones, J. Wu, Y. Li, S. Zhang, J. Ho, B. M. Davis, K. M. Albers, D. H. Kaplan, Cutaneous $TRPV1^+$ neurons trigger protective innate Type 17 anticipatory immunity. *Cell* **178**, 919–932 e14 (2019).
63. L. Jin, L. Ghimire, S. Paudel, S. Cai, T. Rangasamy, S. Jeyaseelan, $MCP\text{-}_1$ plays a critical role in neutrophil function and pyroptosis during Carbapenemf-Resistant *Klebsiella Pneumoniae*. *J. Immunol.* **200**, 46.17 (2018).
64. A. I. Caceres, M. Brackmann, M. D. Elia, B. F. Bessac, D. del Camino, M. D'Amours, J. S. Witek, C. M. Fanger, J. A. Chong, N. J. Hayward, R. J. Homer, L. Cohn, X. Huang, M. M. Moran, S. E. Jordt, A sensory neuronal ion channel essential for airway inflammation and hyperreactivity in asthma. *Proc. Natl. Acad. Sci. U.S.A.* **106**, 9099–9104 (2009).
65. A. Wallrapp, S. J. Riesenfeld, P. R. Burkett, R. E. Abdulnour, J. Nyman, D. Dionne, M. Hofree, M. S. Cuoco, C. Rodman, D. Farouq, B. J. Haas, T. L. Tickle, J. J. Trombetta, P. Baral, C. S. N. Klose, T. Mahlakoiv, D. Artis, O. Rozenblatt-Rosen, I. M. Chiu, B. D. Levy, M. S. Kowalczyk, A. Regev, V. K. Kuchroo, The neuropeptide NMU amplifies ILC2-driven allergic lung inflammation. *Nature* **549**, 351–356 (2017).
66. B. B. Ural, S. T. Yeung, P. Damani-Yokota, J. C. Devlin, M. de Vries, P. Vera-Licona, T. Samji, C. M. Sawai, G. Jang, O. A. Perez, Q. Pham, L. Maher, P. Loke, M. Dittmann, B. Reizis, K. M. Khanna, Identification of a nerve-associated, lung-resident interstitial macrophage subset with distinct localization and immunoregulatory properties. *Sci. Immunol.* **5**, eaax8756 (2020).
67. S. Chakarov, H. Y. Lim, L. Tan, S. Y. Lim, P. See, J. Lum, X. M. Zhang, S. Foo, S. Nakamizo, K. Duan, W. T. Kong, R. Gentek, A. Balachander, D. Carbajo, C. Bleriot, B. Malleret, J. K. C. Tam, S. Baig, M. Shabeer, S. E. S. Toh, A. Schlitzer, A. Larbi, T. Marichal, B. Malissen, J. Chen, M. Poidinger, K. Kabashima, M. Bajenoff, L. G. Ng, V. Angeli, F. Ginhoux, Two distinct interstitial macrophage populations coexist across tissues in specific subtissular niches. *Science* **363**, eaau0964 (2019).
68. V. A. Pavlov, W. R. Parrish, M. Rosas-Ballina, M. Ochani, M. Puerta, K. Ochani, S. Chavan, Y. Al-Abed, K. J. Tracey, Brain acetylcholinesterase activity controls systemic cytokine levels through the cholinergic anti-inflammatory pathway. *Brain Behav. Immun.* **23**, 41–45 (2009).
69. V. A. Pavlov, S. S. Chavan, K. J. Tracey, Molecular and functional neuroscience in immunity. *Annu. Rev. Immunol.* **36**, 783–812 (2018).
70. L. Jia, S. Lee, J. A. Tierney, J. K. Elmquist, M. D. Burton, L. Gautron, TLR4 signaling selectively and directly promotes CGRP release from vagal afferents in the mouse. *eNeuro* **8**, 10.1523/ENEURO.0254-20.2020 (2021).
71. F. De Logu, R. Nassini, A. Hegron, L. Landini, D. D. Jensen, R. Latorre, J. Ding, M. Marini, D. S. M. de Araujo, P. Ramirez-Garcia, M. Whittaker, J. Retamal, M. Titiz, A. Innocenti,

T. P. Davis, N. Veldhuis, B. L. Schmidt, N. W. Bunnett, P. Geppetti, Schwann cell endosome CGRP signals elicit periorbital mechanical allodynia in mice. *Nat. Commun.* **13**, 646 (2022).
72. A. M. Grandits, R. Wieser, Gene expression changes contribute to stemness and therapy resistance of relapsed acute myeloid leukemia: Roles of *SOCS2*, *CALCRL*, *MTSS1*, and *KDM6A*. *Exp. Hematol.* **99**, 1–11 (2021).
73. C. M. Davenport, B. J. W. Teubner, S. B. Han, M. H. Patton, T. Y. Eom, D. Garic, B. J. Lansdell, A. Shirinifard, T. C. Chang, J. Klein, S. M. Pruett-Miller, J. A. Blundon, S. S. Zakharenko, Innate frequency-discrimination hyperacuity in Williams-Beuren syndrome mice. *Cell* **185**, 3877–3895. e21 (2022).
74. M. Zelikowsky, M. Hui, T. Karigo, A. Choe, B. Yang, M. R. Blanco, K. Beadle, V. Gradinaru, B. E. Deverman, D. J. Anderson, The neuropeptide Tac2 controls a distributed brain state induced by chronic social isolation stress. *Cell* **173**, 1265–1279. e19 (2018).
75. N. Sun, L. Yu, Y. Gao, L. Ma, J. Ren, Y. Liu, D. S. Gao, C. Xie, Y. Wu, L. Wang, J. Hong, M. Yan, MeCP2 epigenetic silencing of *Oprm1* gene in primary sensory neurons under neuropathic pain conditions. *Front. Neurosci.* **15**, 743207 (2021).
76. C. Yan, T. Zeng, K. Lee, M. Nobis, K. Loh, L. Gou, Z. Xia, Z. Gao, M. Bensellam, W. Hughes, J. Lau, L. Zhang, C. K. Ip, R. Enriquez, H. Gao, Q. P. Wang, Q. Wu, J. J. Haigh, D. R. Laybutt, P. Timpson, H. Herzog, Y. C. Shi, Peripheral-specific Y1 receptor antagonism increases thermogenesis and protects against diet-induced obesity. *Nat. Commun.* **12**, 2622 (2021).
77. Y. W. Dai, J. K. Ma, R. Jiang, X. L. Zhan, S. Y. Chen, L. L. Feng, Q. Zhang, T. B. Liang, K. Lv, G. J. Yang, J. F. Lu, J. Chen, X. J. Lu, Meteorin links the bone marrow hypoxic state to hematopoietic stem/progenitor cell mobilization. *Cell Rep.* **40**, 111361 (2022).

Acknowledgments: We thank L. Gautron (The University of Texas Southwestern Medical Center) and M. D. Burton (University of Texas at Dallas) for suggestions in VG organotypic culture. We thank S. P. Devkota for assistance in VG isolation and members of the Baral Lab for helpful discussions. We thank S. Fleming for reading the manuscript and providing comments and feedback. We extend thanks to B. Pokhrel and P. Aryal for moral support during the entire project. We also thank S. L. Park and J. Sanneman for technical support. Figures 1, 6, 7, 8, and 9 were created with BioRender.com. **Funding:** This work was supported by funding from NIH/NIGMS P20GM113117 (to P.B.) and the American Lung Association, grant number 1036079 (to P.B.). We acknowledge Johnson Cancer Research Center (JCRC) for providing Linders Family Expansion Award (to P.B.) and Heart Research Award (to P.R.J.), and K-INBRE scholarship to C.C. and A.J. **Author contributions:** Conceptualization: P.B. Methodology: P.B., P.R.J., S.A., and M.M. Investigation: P.R.J., S.A., C.O., C.C., A.J., and P.B. Formal analyses: P.B., P.R.J., S.A., and C.O. Visualization: P.B. and P.R.J. Supervision: P.B. Funding acquisition: P.B. Resources: P.B. and M.M. Project administration: P.B. and P.R.J. Writing—original draft: P.R.J. and P.B. Writing—review and editing: P.R.J. and P.B. **Competing interests:** The authors declare that they have no competing interests. **Data and materials availability:** All data needed to evaluate the conclusions in the paper are present in the paper and/or the Supplementary Materials.

Submitted 1 November 2023
Accepted 30 July 2024
Published 6 September 2024
10.1126/sciadv.adl6162